

1 **Optimization of Thermo-Optical Properties of SiO₂/Ag–CuO Nanofluid for**
2 **Direct Absorption Solar collectors.**

3 Albin Joseph^a, Sreehari Sreekumar^b, C.S.Sujith Kumar^b, Shijo Thomas^{a*}

4 ^a School of Materials Science and Engineering, National Institute of Technology, Calicut
5 673601, India.

6 ^b Department of Mechanical Engineering, National Institute of Technology, Calicut 673601,
7 India.

8 *Corresponding Author: Shijo Thomas, Email Address: shijo@nitc.ac.in

9 **ABSTRACT**

10 Augmenting thermal and optical properties of working fluids used in solar thermal
11 conversion systems using hybrid nanomaterials is gaining prominence. In the present study
12 photo-thermal analysis and thermal conductivity investigations were performed on SiO₂/Ag-
13 CuO binary water based nanofluid. The influence of particle concentration and surfactant
14 concentration on thermo-optical properties were investigated using the design of experiment
15 concept. Analysis of variance (ANOVA) was employed to study the significance of the process
16 parameters on thermal conductivity and solar weighted absorption fraction of nanofluid. The
17 statistical optimisation of the process parameters was done using the desirability function. The
18 optimum combination of nanoparticles and surfactant that yield good thermal conductivity and
19 solar absorption was found to be SiO₂/Ag: 206.3 mg/litre, CuO: 864.7 mg/litre, and SDS
20 (surfactant): 1996.2 mg/litre. The optimum mass fraction of constituents yielded a relative
21 thermal conductivity of 1.234 and solar weighted absorption fraction of 82.82 %.

22 Keywords: Binary nanofluid, SiO₂/Ag particles, CuO nanoparticles, Thermal conductivity,
23 solar weighted absorption fraction, solar thermal conversion.

24
25 **Nomenclature**

A_m	Solar weighted absorption fraction	Q	Photo thermal conversion rate (J)
$A(\lambda)$	Solar absorption coefficient	CCD	Central composite design
C_p	Specific heat (kJ/Kg.K)	DoE	Design of experiments
$I(\lambda)$	Spectral solar irradiance (w/m ² nm)	RSM	Response surface methodology

m	Mass (kg)	RTC	Relative thermal conductivity
Tr	Transmittance	SDS	Sodium dodecyl sulphate
Ti	Initial Temperature (°C)	SWAF	Solar weighted absorption fraction
Ts	Final Temperature (°C)		

26

27

1. INTRODUCTION

28

29

30

31

32

33

34

35

36

37

38

39

40

41

42

43

44

45

46

47

48

49

50

Renewable energy have gained wide attention due to the growing demand of clean and economical energy resources. Among various renewable energy sources like wind, solar, tide etc., solar energy is found to be one of the most promising candidate due to its abundant availability. Current trend in utilising solar energy is mainly through photo-voltaic conversion, photo thermal conversion, and photochemical conversion. Among these techniques photo thermal conversion is the most efficient method. When coupled with a thermal storage system, it ensure round the clock thermal energy supply [1]. Solar thermal conversion can be achieved by concentrating and non-concentrating modes, among which concentrating solar thermal systems are found to more effective [2, 3]. Concentrating solar thermal conversion mainly involves four major steps: i) tracking and concentrating solar rays onto a solar receiver, ii) conversion into useful heat energy by means of absorber unit, iii) transferring heat from absorber to heat transfer fluid, and iv) adiabatic storage of fluid. Among these four steps the efficiency of a solar thermal system depends on the performance of stage two and three, i.e. absorption and transfer of the absorbed energy. Hence the primary focus of current researches is to enhance the thermo-optical properties of the absorbing and transferring units in the system. A conventional solar absorber converts solar energy to heat energy which then is transferred to heat transfer fluid (working fluid) by conduction, followed by convection, resulting in a temperature drop across the absorber surface [4]. Absorption of solar radiation directly by the working fluid could reduce the intermediate thermal losses associated with the conventional solar absorber [5]. However, the conventional working fluids like water, thermal oils, glycol etc. are not suitable for direct solar absorption due to their poor optical and thermal properties. It is reported that dispersion of nanoparticles in working fluid improves its optical and thermal properties which makes it suitable for direct solar absorption [6, 7].

51

52

53

Since 1990s nanofluids were extensively employed for thermal transport due to its enhanced thermal properties. A systematic review done by Mahian et al. [38, 39] explores the potential, theory and mechanism of nanofluids responsible for the enhancement in the

54 properties. Sarfraz and Safaei [43] investigated the effect of graphene-menthanol based
55 nanofluid on evacuated tube solar collector. The authors achieved a maximum efficiency of
56 95% due to the enhancement on the thermal conductivity of the nanofluid. They also concluded
57 that since Brownian motion is the phenomenon responsible for higher thermal conductivity of
58 the nanofluids, they are suitable for various heat transfer applications. The progress in
59 technologies made it feasible to enhance the performance of solar thermal devices like
60 parabolic collector, solar stills, flat plate collector, hybrid PV/ Thermal collectors, direct solar
61 steam generators, etc. with the aid of nanofluids [33, 34]. However, most of the initial
62 investigations were focused on nanofluids containing single nanoparticle that includes metal
63 (Cu, Al, Ag, Au etc.), metal oxides (CuO, Al₂O₃, TiO₂, etc.), etc. [8, 9, 10]. Furthermore carbon
64 based nanofluids, multi walled CNT, single walled CNT, graphene oxide, and graphene Nano
65 platelets are found to be potential candidates for solar thermal application due to their
66 favourable optical properties [32]. Later investigations reported that hybrid nanofluids could
67 exhibit better properties due to the interacted effect of more than one nanoparticle [11, 12].
68 Recently Yu and Xuan [13] studied the influence of CuO/Ag hybrid nanofluid on the
69 absorption of solar irradiance. The authors concluded that the CuO/Ag nanoparticles exhibits
70 a notable enhancement in thermal conductivity and photo thermal performance of the base
71 fluid. The enhancement in solar absorptivity is attributed to the localised surface plasmon
72 resonance (LSPR) effect of Ag nanoparticles when exposed to solar irradiance. Later reports
73 of J Zeng and Y Xuan [14] arrived at similar conclusions while using SiO₂/Ag-MWCNT hybrid
74 nanofluid as the medium of solar absorption, with SiO₂/Ag giving wide absorbance spectrum
75 in visible region and MWCNT in infrared. The authors also claim that MWCNT when
76 dispersed in base fluid improved the thermal conductivity of the hybrid nanofluid. The effect
77 of particle shape on solar absorptivity was investigated by Qin et al. [37]. The authors
78 concluded that the particle with sharper edges exhibits better absorption due to the combined
79 effect of surface plasmon resonance and lightning rod effect. Bhalla et al. [35] conducted an
80 interesting study to enhance the absorption in the mod infrared region. The authors introduced
81 silicon oil layer above the nanofluid having high absorptivity in the visible region. The unique
82 property, high transmittance of visible rays and absorptivity in infrared region was utilised for
83 the full spectrum absorption of solar energy in the system. The effect of crystallite size of
84 nanoparticle on its properties was investigated by J Shah et al. [44]. The authors synthesised
85 CuO nano particles with various shape and crystallite shape and concluded that better
86 absorption was noted for nanorod in the visible region. Enhanced photo thermal conversion
87 was noted for FeNi/C based nanofluid under a magnetic rotation for direct absorption of solar

88 irradiance [45]. Photo thermal conversion efficiency of rotating nanofluid enhanced by 22.7%
89 compared to the non-rotational field of solar irradiation. The reason behind this was attributed
90 to the enhanced convection heat transfer during the rotation of nanofluid. The effect of carbon
91 on solar thermal conversion was studied by S. K. Hazra et al. [46]. A maximum optical
92 absorptivity of 87.33% with a penetration depth of 20mm was noted at 15 ppm of carbon black.
93 K. Wang et al. [47] proposed that a direct absorption system integrated with Rayleigh-Benard
94 convection could exhibit a significant enhancement in the photo thermal conversion of the
95 system. This is due to the increased heat transfer by convection within the nanofluid.

96 From the literature it is noticed that localised plasmonic resonance effect of noble
97 metals is a desired phenomenon that could be adopted for enhanced optical properties of
98 nanofluids. Nevertheless it was found that the hybrid nanoparticles are large in size that
99 adversely affect the stability and thus the properties of the nanofluid [14]. O.Z Sharaf et al. [48]
100 developed a highly stable polyethylene glycol coated gold nanoparticle based nanofluid. The
101 synthesised nanofluid exhibited an extra ordinary stability of 16 months that could guarantee
102 the repeatability of its properties. K. Pawel et al [15] reports that size of the particle have very
103 high significance in improving thermal properties like thermal conductivity of nanofluid.
104 According to his investigation better thermal conductivity was observed for nanofluid with
105 smaller materials. Due to these reason it could be speculated that large sized (>100 nm) hybrid
106 nanoparticles could not provide consistent and notable enhancement in thermal properties of
107 nanofluid. Since CuO nanoparticles of size less than 50 nm are a good candidate to improve
108 thermal conductivity, it has been widely used for thermal transport [16]. In addition,
109 investigations on CuO nanofluid shows positive results for enhanced thermal and optical
110 properties [17].

111 To explore the complex interaction of various process parameters on output response,
112 varying one parameter at a time is not a suitable approach. In such multivariate situations,
113 design of experiments (DoE), artificial neural network and fuzzy logic are the widely
114 acknowledged technique employed for the same. Among these techniques, design of
115 experiments is the most adaptable technique that could provide a clear picture about interaction
116 of process variables involved in the study and its response with least number of experimental
117 runs [18].

118 Present investigation aims to synthesise, optimise and characterise SiO₂/Ag-CuO
119 hybrid nanofluid where SiO₂/Ag nanoparticles are a good candidate to absorb the solar

120 radiation and CuO as an agent to improve the thermal conductivity. Design Expert software
121 was employed to generate design matrix based on the design of experiments concept. In the
122 present study, response surface methodology was adopted to analyse the complex interaction
123 of various process variable (or process parameters) on output response (solar weighted
124 absorption fraction and thermal conductivity are the output response in the present study).
125 Further, the thermal conductivity and solar weighted absorption fraction of the synthesised
126 hybrid nanofluid was measured experimentally based on the design matrix. Finally a
127 mathematical model was developed for the prediction of thermal conductivity and solar
128 weighted absorptivity as a function of mass fraction of SiO₂/Ag, CuO and surfactant.
129 Nevertheless no available reports describing the use of SiO₂/Ag-CuO binary nanofluid for
130 photo thermal conversion studies by employing DoE.

131 **2. Materials and methods**

132 *2.1 Materials*

133 The precursor used for the synthesis of SiO₂ was Tetraethyl orthosilicate (TEOS) (Alfa
134 Aeser). Ammonia solution, ethanol, Stannous chloride (SnCl₂) (reducing agent) and CuO nano
135 particles (size<50nm) purchased from Sigma Aldrich were used directly with no further
136 purification. Silver nitrate (AgNO₃) (Sigma Aldrich) was used as precursor for silver
137 nanoparticle.

138 *2.2 Preparation of SiO₂/Ag nanoparticle*

139 Stober method [19] was adopted for synthesising SiO₂ nanoparticles. 3 ml TEOS, 100
140 ml ethanol, 6 ml ammonium hydroxide and 6 ml DI water were taken and stirred for five hours
141 continuously. From the resulting mixture, SiO₂ nanospheres was separated by centrifugation,
142 and washed five times with DI water. Silver particles were introduced onto the silica
143 nanosphere by following reaction: SnCl₂ (0.053 M) and hydrochloric acid (0.01 M) were mixed
144 in 40 ml of DI water into which 0.15 g of synthesised SiO₂ was added. This mixture is then
145 stirred for 20 minutes followed by rinsing with DI water for 5 times. The resulting solution is
146 then added to 40 ml silver nitrate solution (0.18 M) and sonicated for 30 minutes to induce Ag
147 particles on the silica sphere. Finally SiO₂/Ag nanoparticles were separated by filtering through
148 centrifugation, which was then cleaned and rinsed with DI water for 5 times.

149 *2.3 Preparation of SiO₂/Ag-CuO nanofluid*

150 Literature reveals that the properties of nanofluid depends on the various process
151 parameters involved in the synthesis of nanofluid [20]. In the present investigation, three
152 process parameters, viz. mass fractions of SiO₂/Ag, CuO and SDS (surfactant), were identified
153 as the process parameters which influence the output responses. The output responses are
154 thermal conductivity and the solar weighted absorption fraction. Since there are more than one
155 process parameter involved, varying one parameter-at-a-time and analysing its effect on the
156 thermal conductivity and solar weighted absorption fraction of nanofluid is time consuming
157 and expensive [18]. Hence, in order to analyse the complex interaction of these process
158 parameters on the output response, design of experiments (DoE) concept was adopted. Design
159 of experiments is a collection of tools used mainly to interpret the influence of process
160 parameters on output response [41]. Among the various tools in DoE, response surface
161 methodology was employed [21] in the present study to analyse the influence of variation in
162 process variables on thermo-optical properties (thermal conductivity and solar weighted
163 absorption fraction) of the nanofluid. The workable range of the process parameters (mass
164 fractions of SiO₂/Ag, CuO and surfactant) were fixed based on the literature survey and
165 preliminary experimental trials. The workable range is the upper and lower value of process
166 parameters on which a feasible nanofluid was synthesised. In the present study the surfactant
167 used was sodium dodecyl sulphate (SDS), for which the critical micelle concentration (CMC)
168 was found to be 8.2 mM at 25°C. Since the recommended usage of surfactant is below the
169 CMC, the upper limit of mass fraction of surfactant was taken as 2000 mg/l. The mass fraction
170 limit of SiO₂/Ag, CuO and SDS were fixed as 100 -1500 mg/l, 100 -1500 mg/l, and 100-
171 2000mg/l, respectively. Based on these limits a design matrix with 20 set of experimental runs
172 were generated using the Design Expert software, as shown in Table 1.

173 Based on the combination of process parameters arrived using DOE, the nanoparticles
174 and surfactant were dispersed in 40 ml of DI water followed by mechanical agitation for 30
175 minutes and 15 minutes of sonication. In the present study probe sonication was adopted as it
176 is reported in literature [36] to be best suited for preparation of nanofluids. Once the nanofluid
177 samples based on the design matrix is prepared, its thermal conductivity and solar weighted
178 absorption fraction were measured. Based on these results, models were developed for thermal
179 conductivity and solar weighted absorption fraction as function of the process parameters. The
180 suitability of the developed models and the significance of the process parameters were
181 analysed using the analysis of variance (ANOVA) of response surface methodology (RSM).

182 **Table 1:** Design matrix for the experiments to be conducted.

Run No	SiO ₂ /Ag (mg/l)	CuO (mg/l)	Surfactant (mg/l)
1	800.0	800.0	1050.0
2	383.8	1216.2	1614.9
3	100.0	800.0	1050.0
4	1216.2	1216.2	1614.9
5	800.0	800.0	1050.0
6	1216.2	1216.2	485.1
7	800.0	800.0	1050.0
8	800.0	1500.0	1050.0
9	383.8	383.8	1614.9
10	383.8	383.8	485.1
11	1216.2	383.8	485.1
12	383.8	1216.2	485.1
13	1216.2	383.8	1614.9
14	800.0	800.0	1050.0
15	1500.0	800.0	1050.0
16	800.0	100.0	1050.0
17	800.0	800.0	1050.0
18	800.0	800.0	2000.0
19	800.0	800.0	1050.0
20	800.0	800.0	100.0

183

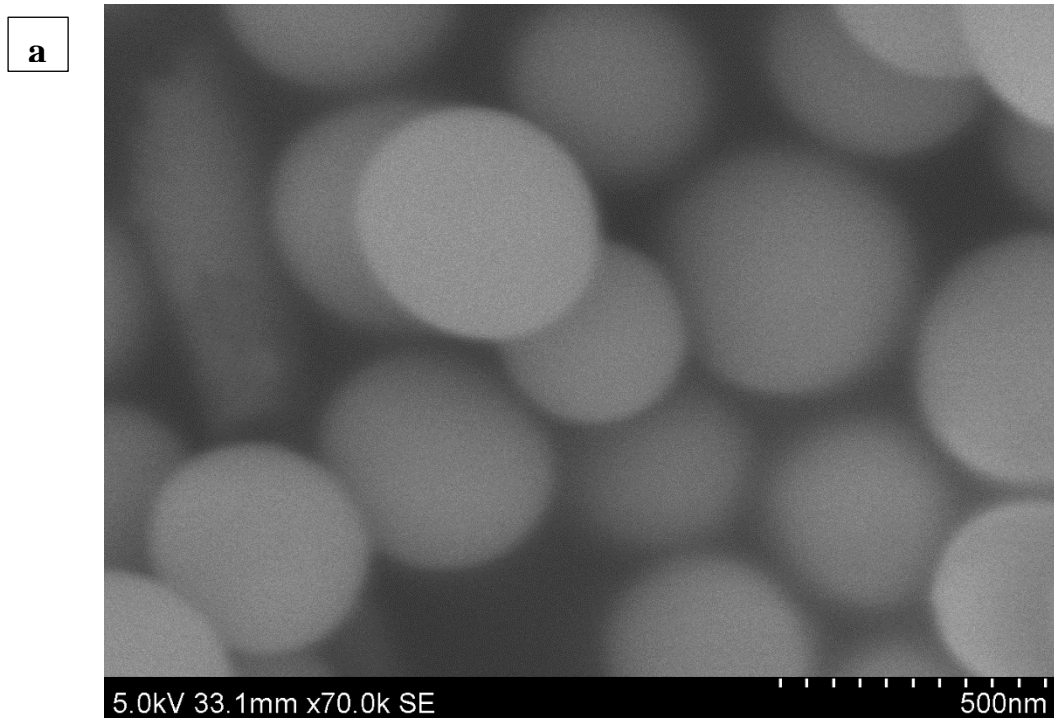
184 **3. Results and Discussion**

185 *3.1 Characterisation*

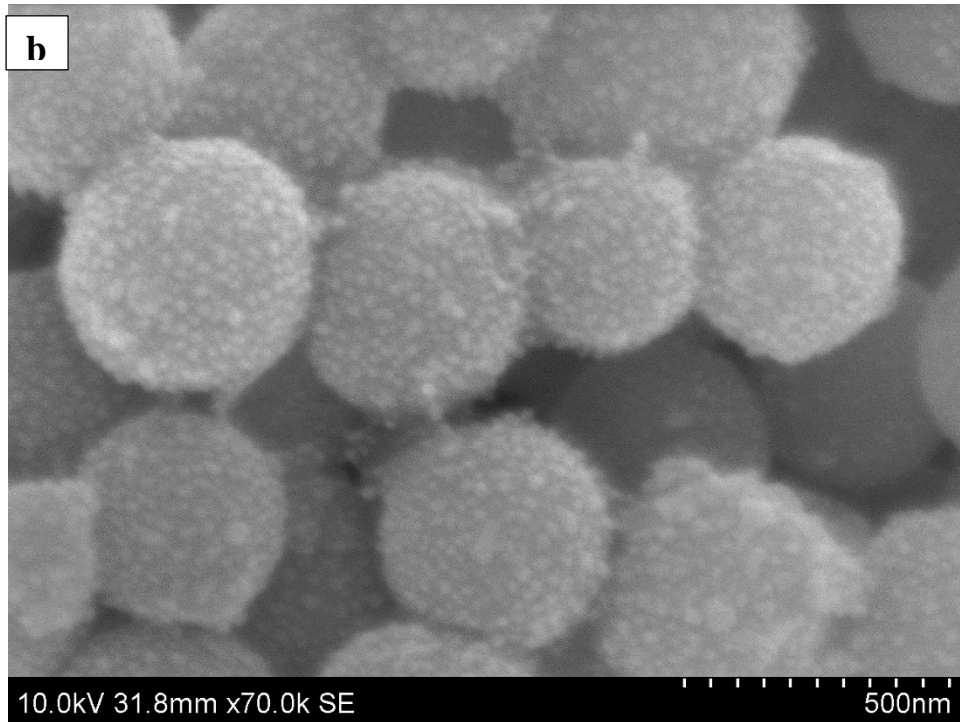
186 Morphological analysis of the nanoparticles were carried out using field emission
187 scanning electron microscope (FESEM) (Hitachi SU 6600). UV-VIS Spectroscopic (Avantes)
188 analysis from 280-1200 nm was carried out at atmospheric condition to analyse the absorptivity
189 of the nanofluid at various wavelength. Air was considered as the reference for measuring the
190 absorptivity of the nanofluid. KD2 Pro analyser (Decagon Devices Inc) was employed to
191 estimate the thermal conductivity of nanofluid. Each measurement was repeated thrice to
192 ensure repeatability. Uncertainty of the KD2 Pro analyser is $\pm 2.5\%$ [22]. It is obvious that the
193 properties of nanofluid which is measured soon after preparation could not be expected during
194 the applied experimentation due to the variation of stability with samples. Due to this reason
195 all the properties were measured after 50 hours of preparation. The optical properties were
196 quantified in terms of the solar weighted absorption fraction (SWAF). The SWAF was arrived
197 at from the transmittance spectrum obtained using UV-vis spectroscopy (Avantes).

198 *3.1.1 Morphology of the particles*

199 The morphological analysis of the SiO₂ and SiO₂/Ag was performed using a Scanning
200 electron microscope and is shown in Fig 1. Figure 1a and 1b shows the pure SiO₂ particles and
201 SiO₂/Ag particles respectively. The deposition of Ag particles on the surface of the SiO₂
202 particles is clear from the figure 1b. In addition, from these figures it is clear that the SiO₂
203 nanoparticles exhibit homogenous shape and size, and hence are favourable for the deposition
204 of smaller particles [14]. The average particle size was found to be 300 nm. The Ag
205 nanoparticles were deposited on SiO₂ using the reducing agent SnCl₂. Figure 2 shows the
206 mechanism involved in the deposition of Ag on SiO₂ nanoparticles using the reducibility of
207 Sn²⁺ ions. Sn²⁺ ions were introduced on to the SiO₂ which is then replaced by Ag particles on
208 reacting with AgNO₃.



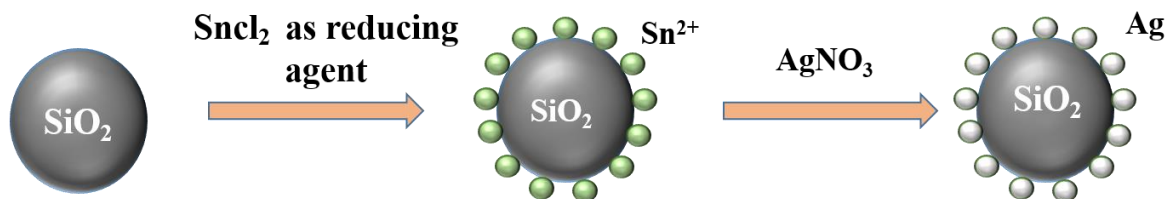
209



210

211 **Fig. 1:** a) SEM image of SiO₂ nanoparticles, b) SEM images of SiO₂/Ag nanoparticles

212



213

214 **Fig. 2:** Schematic representation of the synthesis of SiO₂/Ag nanoparticles.

215

216 *3.1.2 Thermal conductivity analysis*

217 KD2 Pro Thermal property analyser was employed to analyse the thermal conductivity
 218 of the synthesised samples. Table 2 shows the relative thermal conductivity (RTC) experienced
 219 by the nanofluids at 28°C. As can be seen in Table 2, the addition of nanoparticles improved
 220 the thermal conductivity of the base fluid. However, variation in the concentration of SiO₂/Ag
 221 and CuO have an influence on the thermal conductivity of nanofluid. Run no 2 shows the
 222 maximum enhancement of 23.35 % (RTC = 1.2335) for thermal conductivity while run no 20
 223 gives the least. It is also noted from run 9 and 13 that as the concentration of SiO₂/Ag decreases
 224 the thermal conductivity increases. In addition, thermal conductivity exhibited by the nanofluid
 225 was found to be increased with the concentration of CuO (run 2 and 9). Therefore it could be

226 surmised that the enhanced thermal conductivity is obtained at lower concentration of SiO₂/Ag
 227 and higher concentration of CuO.

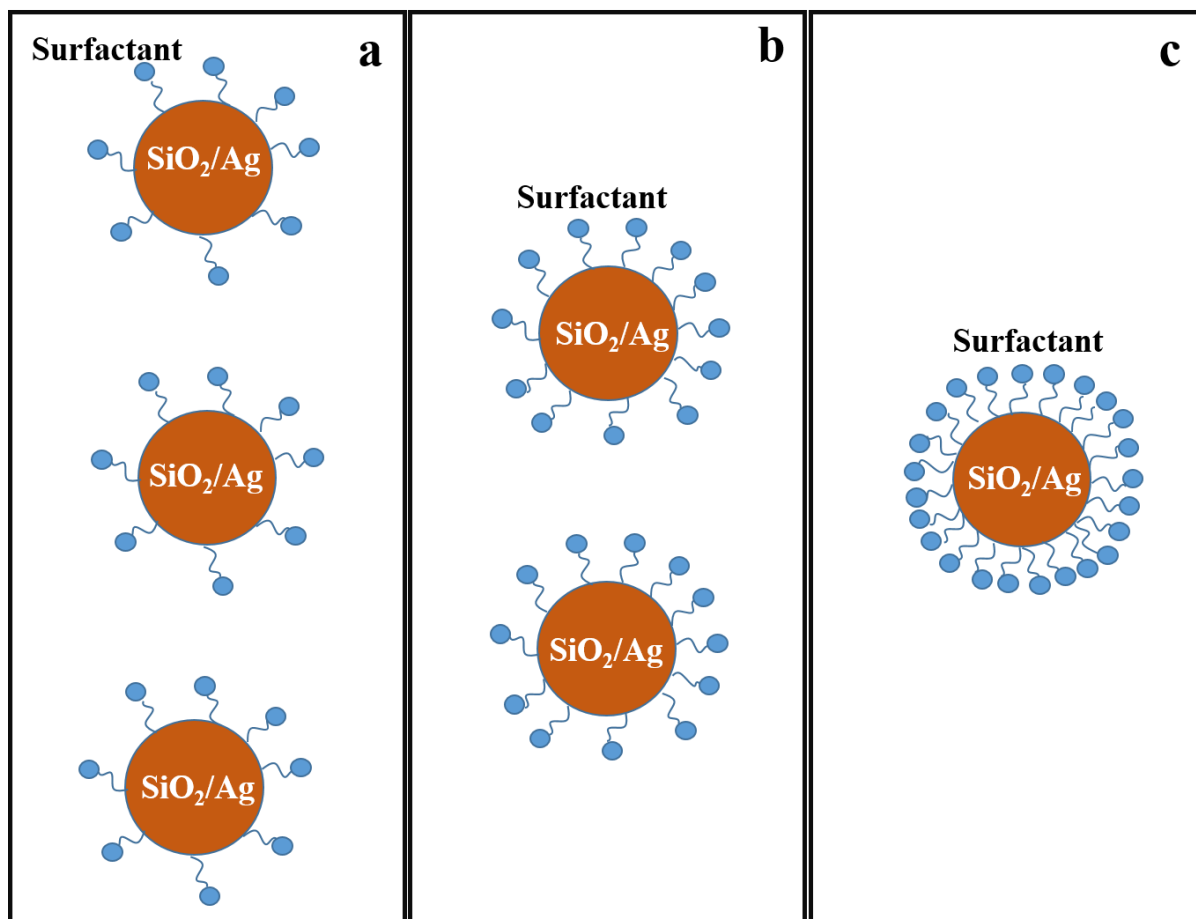
228 **Table 2:** Design matrix with output response

Run	Mass Fraction			Solar Weighted absorption fraction (%)	Relative Thermal Conductivity
	A:SiO ₂ /Ag (mg/l)	B:CuO (mg/l)	C:SDS (mg/l)		
1	800.0	800.0	1050.0	73.2	1.1261
2	383.8	1216.2	1614.9	79.75	1.2335
3	100.0	800.0	1050.0	70.33	1.2051
4	1216.2	1216.2	1614.9	71.18	1.1789
5	800.0	800.0	1050.0	71.2	1.1416
6	1216.2	1216.2	485.1	62.7	1.0981
7	800.0	800.0	1050.0	74.2	1.1574
8	800.0	1500.0	1050.0	69.17	1.1598
9	383.8	383.8	1614.9	82.82	1.1448
10	383.8	383.8	485.1	61.96	1.1159
11	1216.2	383.8	485.1	61.99	1.0948
12	383.8	1216.2	485.1	65.05	1.1463
13	1216.2	383.8	1614.9	76.51	1.1021
14	800.0	800.0	1050.0	75.2	1.1358
15	1500.0	800.0	1050.0	62.82	1.1041
16	800.0	100.0	1050.0	72.74	1.1126
17	800.0	800.0	1050.0	74.2	1.1328
18	800.0	800.0	2000.0	79.77	1.1789
19	800.0	800.0	1050.0	72.2	1.1486
20	800.0	800.0	100.0	50.87	1.0659

229

230 For a fixed concentration of surfactant and CuO, sedimentation of SiO₂/Ag
 231 nanoparticles was found to be increasing with concentration. Figure 3 shows the distribution
 232 of surfactant molecules on the surface of SiO₂/Ag particles at different concentration. The
 233 concentration of SiO₂/Ag particles decreases from Fig. 3(a) to 3(c). For a given mass fraction
 234 of surfactant, as concentration of SiO₂/Ag particles increases the number of surfactant
 235 molecules per particle will be less, as shown in Fig. 3(a). As the concentration of SiO₂/Ag

236 particles decreases the number of surfactant molecules per particle increases, yielding a more
 237 stable nanofluid as shown in Fig. 3(b) and Fig. 3(c). The reduction in the number of surfactant
 238 molecules per unit nanoparticle may lead to agglomeration and sedimentation, thus decreasing
 239 stability of the nanofluid. SDS being an anionic surfactant, the strength of surface charges on
 240 particle decides the stability of the nanofluid. As the charges on the particle increases, the
 241 repulsion between the particles increases leading to the increased stability.



242
 243 **Fig. 3:** Schematic representation of interaction of surfactant molecules and nanoparticles

244 *3.1.3 ANOVA analysis of thermal conductivity*

245 Analysis of variance (ANOVA) is employed to study level of significance of each
 246 process parameters on output response and to evaluate the model developed. F –value in the
 247 ANOVA table is mainly used to identify the suitability of the model developed and significance
 248 of each process parameters. In the present ANOVA (Table 3) a significant mathematical model
 249 was developed with F-Value 20.47, P-value > 0.0001 and with ‘lack of fit’ of P-value equal to
 250 0.3481. F-Value 20.47 implies that the chance of variation in F-value due to noise is 0.01%,
 251 which implies that the developed model could predict the thermal conductivity of the nanofluid

effectively [31]. Furthermore Pred R² represents the prediction of thermal conductivity based on the arrived model. For an acceptable model the difference between the adjR² and pred R² should be a value between 0 and 2.0 [23], which also confirm that the developed model is suitable for the prediction of thermal conductivity. The final reduced model that predicts the thermal conductivity as a function of mass fraction of nanoparticles and surfactant is given in Eq. 1. In addition, the ANOVA also quantifies the significance of each parameters on the output and is evaluated based on the F-value. The parameter with highest F-value is the most significant parameter. Therefore, as can be seen in Table 3, the most significant parameter that affects thermal conductivity was found to be the concentration of surfactant (F= 72.62), followed by the concentrations of SiO₂/Ag and CuO (F-value 52.89 and 36.26) respectively. From a careful observation of runs 20, 19 and 18 in Table 2, the significance of surfactant in improving the thermal conductivity of nanofluid is evident. The thermal conductivity is found to be low at low surfactant concentrations and high nanoparticle concentrations. Nevertheless it doesn't mean that the increased surfactant concentration gives better thermal conductivity. The surfactant keep the nanoparticles suspended in the fluid which enhances thermophysical properties of the fluid. Furthermore, surfactant-CuO combination shows the most significant interaction (F-value = 13.85) whereas surfactant-SiO₂/Ag gives the least interaction (F-value = 0.63). The reasons for this will be discussed in the section 3.1.4. Figure 4 shows the comparison of predicted (based on Eq. 1) and experimental values of relative thermal conductivity, coloured point represents the experimental data and line shows the predicted values. A significant model exhibits minimum deviation of experimental data points from the prediction line, as is evident in Fig. 4. Hence, the developed model is good enough to predict the thermal conductivity of the prepared nanofluid.

Table 3: ANOVA of thermal conductivity

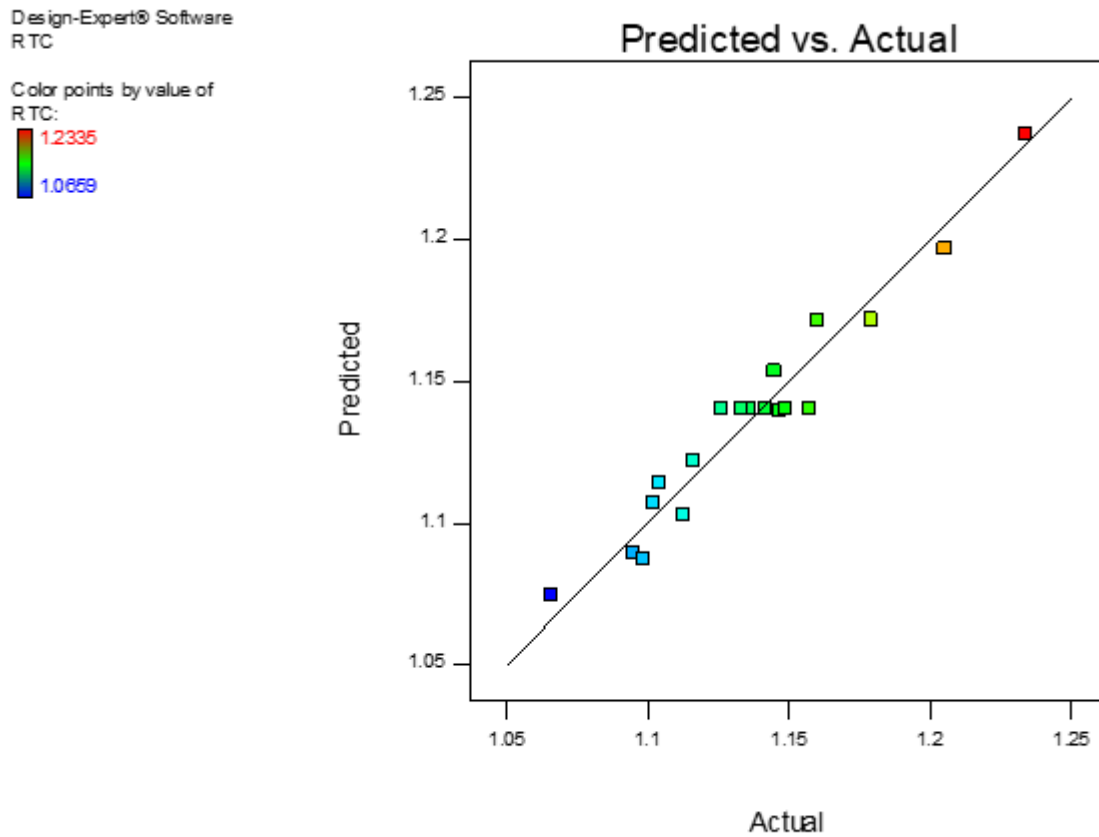
Source	Sum of squares	Df	Mean square	F-value	p-value	
Model	0.029	9	3.208E-003	20.47	< 0.0001	Significant
A-SiO ₂ /Ag	8.289E-003	1	8.289E-003	52.89	< 0.0001	
B-CuO	5.683E-003	1	5.683E-003	36.26	0.0001	
C-SDS	0.011	1	0.011	72.62	< 0.0001	
AB	1.901E-004	1	1.901E-004	1.21	0.2965	
AC	9.800E-005	1	9.800E-005	0.63	0.4474	
BC	2.171E-003	1	2.171E-003	13.85	0.0040	
A ²	4.188E-004	1	4.188E-004	2.67	0.1332	
B ²	1.790E-005	1	1.790E-005	0.11	0.7424	

C^2	5.177E-004	1	5.177E-004	3.30	0.0992	
Residual	1.567E-003	10	1.567E-004			
Lack of Fit	9.262E-004	5	1.852E-004	1.44	0.3481	not significant
Pure Error	6.411E-004	5	1.282E-004			
Cor Total	0.030	19				
Std. Dev.	0.013		R-Squared			0.9485
Mean	1.14		Adj R-Squared			0.9022
C.V. %	1.10		Pred R-Squared			0.7370
PRESS	8.004E-003		Adeq Precision			18.361

276

277 Relative thermal conductivity = $1.11825 - (7.08371E-005 \times \text{SiO}_2/\text{Ag}) + (8.23773E-006 \times$
278 $\text{CuO}) + (4.64016E-005 \times \text{SDS}) - (2.81400E-008 \times \text{SiO}_2/\text{Ag} \times \text{CuO}) - (1.48865E-008 \times$
279 $\text{SiO}_2/\text{Ag} \times \text{SDS}) + (7.00727E-008 \times \text{CuO} \times \text{SDS}) + (3.11178E-008 \times \text{SiO}_2/\text{Ag}^2) - (6.43326E-$
280 $009 \times \text{CuO}^2) - (1.87837E-008 \times \text{SDS}^2)$ (1)

281



282

283 **Fig. 4:** Correlation between experimental and predicted values of relative thermal conductivity
284 of nanofluid.

285

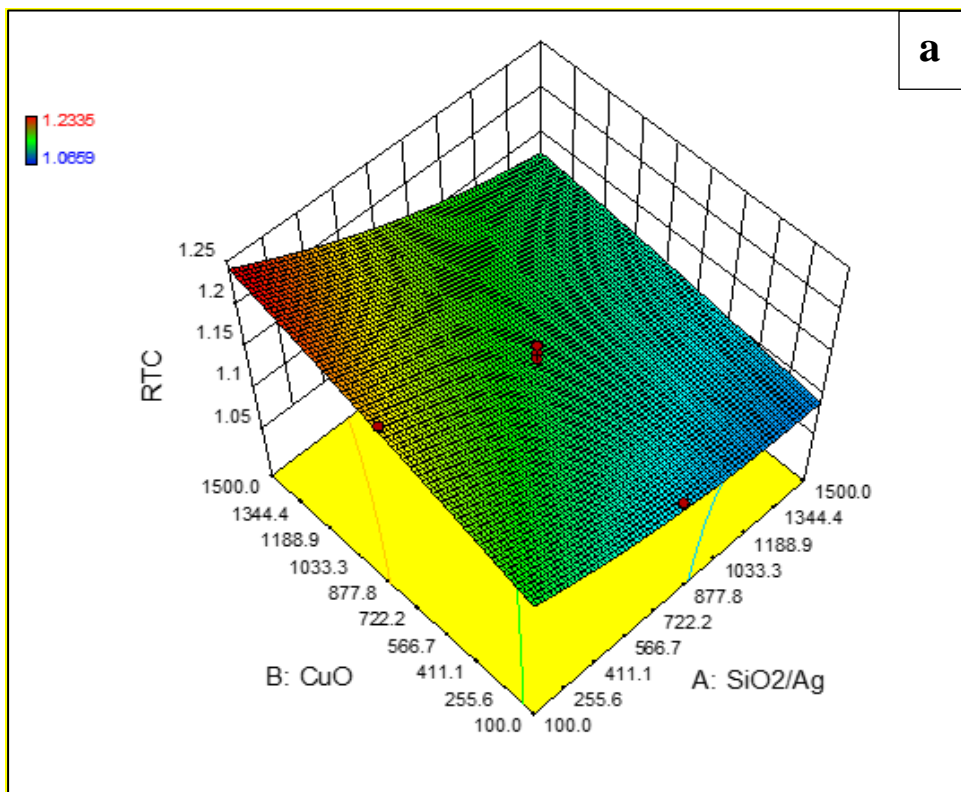
286 3.1.4 Interaction effect of various concentrations of SiO₂/Ag and CuO

287 Figures 5, 6 and 7 gives the interactive effect of two process parameters simultaneously
288 on the response. The interactions are represented as response surfaces (3D interpretation) and
289 contours (2D images). Figure 5a shows the interaction effect of SiO₂/Ag and CuO
290 concentrations on the thermal conductivity of SiO₂/Ag-CuO nanofluid, fig 5b represents its
291 counter plot. It was noticed from figure 5 that at lower concentration of CuO nanoparticles,
292 the thermal conductivity remains almost constant at all SiO₂/Ag concentrations. As evident
293 from Fig. 5, the RTC (relative thermal conductivity) increases significantly with concentration
294 of CuO and the maximum enhancement in relative thermal conductivity was observed at high
295 CuO concentration and low SiO₂/Ag concentration. It is also noticed that at the maximum
296 concentration of CuO, increasing SiO₂/Ag concentration reduces the thermal conductivity. The
297 reason behind this might be the insignificant impact of SiO₂/Ag in improving the thermal
298 conductivity due to the larger size of these particles resulting in lower brownian motion in the
299 nanofluid [15]. The Brownian motion of nanoparticles is considered as one of the prominent
300 mechanisms that enhances the thermal conductivity of nanofluids.

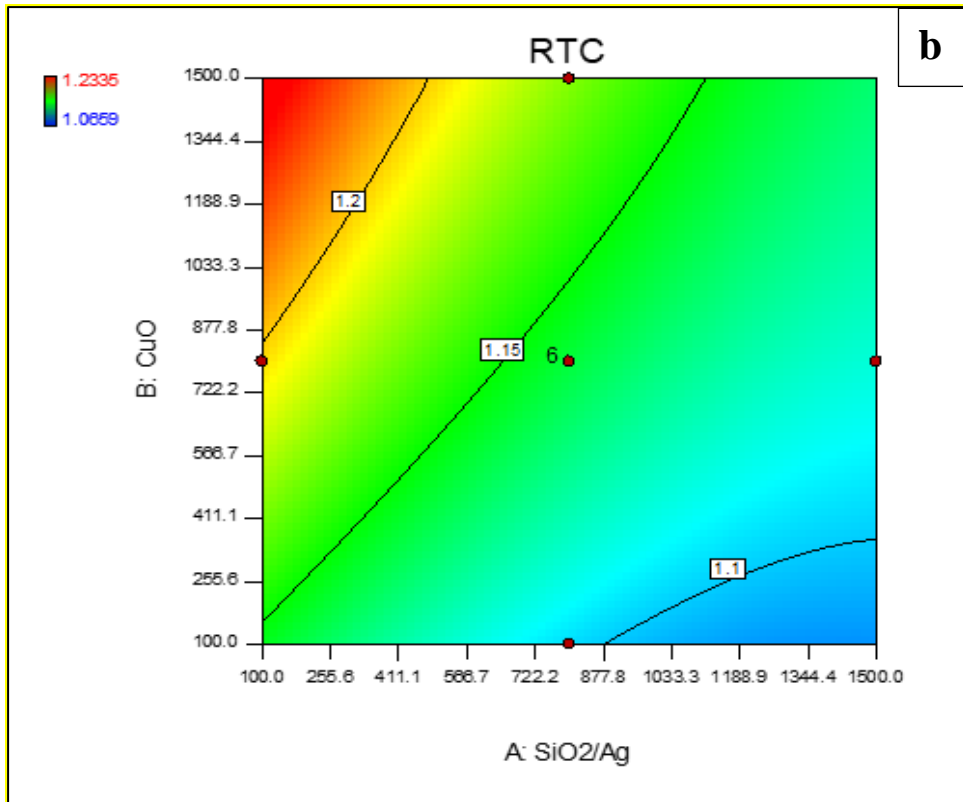
301 Fig 6(a) represents the interaction effects of SDS (surfactant) and SiO₂/Ag using 3D
302 graph, and its contours plot is shown in Fig. 6(b). It is clear from the graphs that the maximum
303 enhancement in the thermal conductivity is at low concentration of the SiO₂/Ag for all
304 concentrations of SDS. This is because, at lower concentrations of SDS the nanoparticles
305 agglomerates, thus lowering the stability and hence the thermal conductivity. At higher
306 concentrations of surfactant the nanofluid was found to be stable. However, at higher
307 concentration of SDS, increasing concentration of SiO₂/Ag reduces number of surfactant
308 molecules per nanoparticles, as shown in Fig.3, which may leads to the agglomeration of
309 nanoparticles and reduction in thermal conductivity. The size of SiO₂/Ag nanoparticles (250 –
310 350 nm) may also have contributed to reduction in thermal conductivity, as literature [15]
311 recommend particle size lower than 100 nm. This may lead to the conclusion that minimum
312 quantity of SiO₂/Ag helps to achieve higher thermal conductivity. However in the present
313 study, in addition to the thermal conductivity, solar absorptivity is also of prime concern. A
314 reduction in the concentration of SiO₂/Ag reduces the optical absorptivity as shown in section
315 3.1.5.

316 Figure 7 shows the interaction effect of concentration of SDS and CuO, Fig 7(a) the
317 response surface plot and Fig 7(b) shows its 2D or contour plot. As can be seen from the figure,

318 the thermal conductivity increases with the concentration of CuO and SDS. Maximum RTC
319 was noted at higher concentration of SDS and CuO results in higher thermal conductivity
320 values. This confirms the significance of CuO to achieve higher thermal conductivity and
321 influence of SDS in offering stability at higher concentration of CuO to achieve improved
322 thermal conductivity.



323

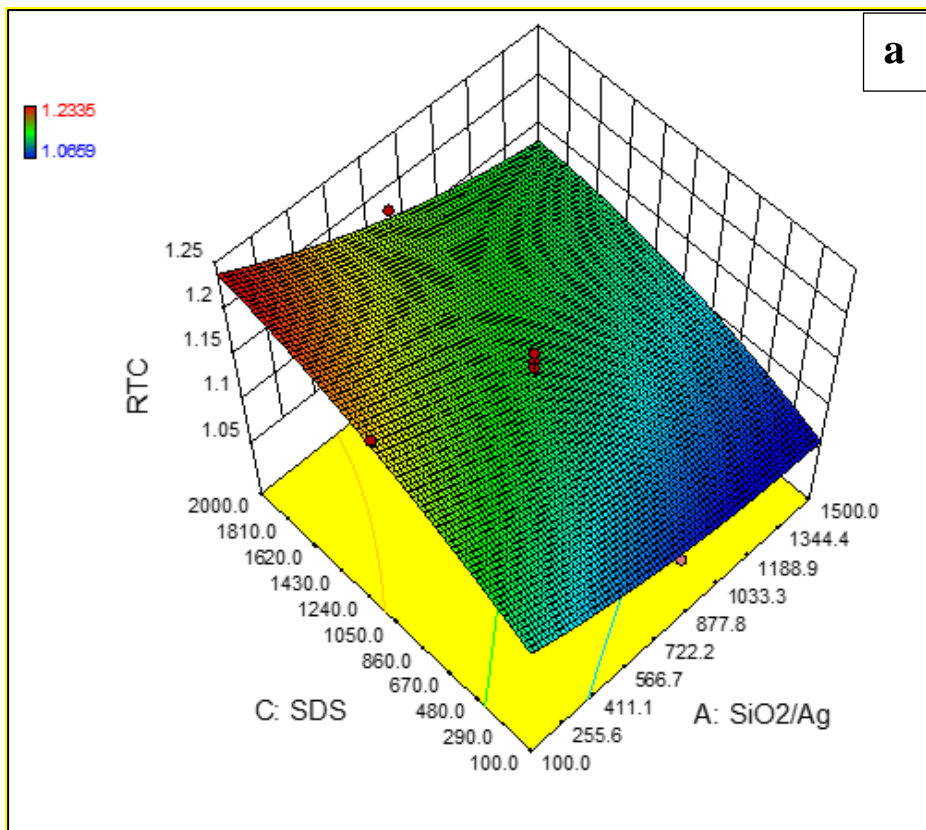


324

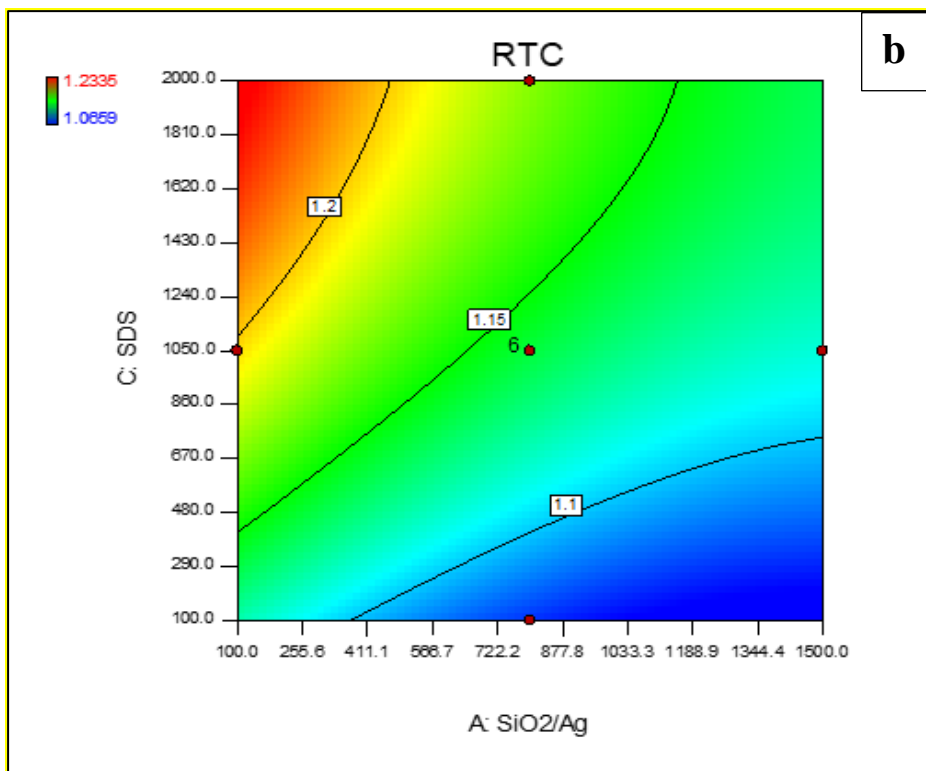
325

326 **Fig. 5:** Interaction effect of concentration of SiO₂/Ag and CuO nanoparticles on relative
 327 thermal conductivity: a) 3-D graph, b) contour plot.

328

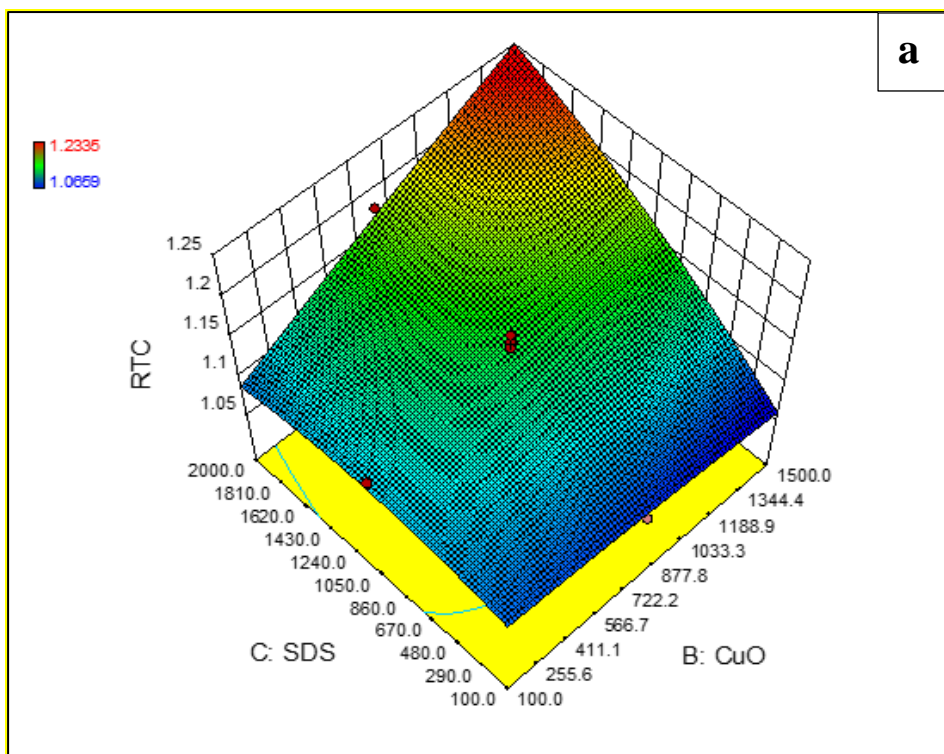


329

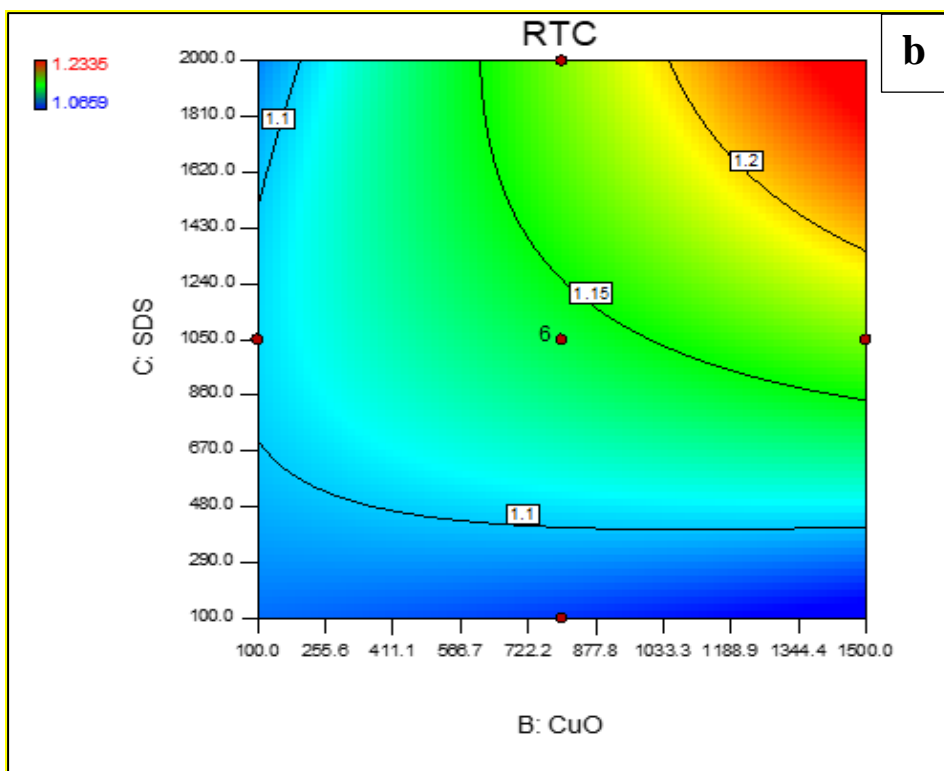


330

331 **Fig. 6:** Interaction effect of SiO₂/Ag and SDS on relative thermal conductivity: a) 3-D graph,
 332 b) contour plot.
 333



334



335

336

337 **Fig. 7:** Interaction effect of concentration of SDS and CuO nanoparticles on relative thermal
 338 conductivity: a) 3-D graph, b) contour plot.

339

340 *3.1.5 Optical properties*

341 Transmittance spectrum of the synthesised nanofluid obtained from the UV-vis
 342 spectroscopy is shown in Fig 8. Transmittance spectrum gives the information on amount of
 343 radiation absorbed by the nanofluid at each wavelength. For a highly absorbing nanofluid the
 344 transmittance will be minimum. Fig 8(a) presents the transmittance spectrum of all the
 345 experimental runs. It could be noticed that run 9 gives the highest absorption of solar irradiance
 346 while run 20 gives the least. A medium solar weighted absorption fraction was observed for
 347 run 12. These runs were selected as the critical runs and are shown in fig 8(b) for better
 348 understanding. To estimate the overall optical absorption rate of the synthesised nanofluid,
 349 solar weighted absorption fraction was calculated using the Eq. (2) given by Drotning [24] and
 350 are presented in table 2.

$$351 \quad A_m = \frac{\int_{\lambda_{min}}^{\lambda_{max}} I(\lambda) \cdot (1 - e^{-A(\lambda) \cdot l}) d\lambda}{\int_{\lambda_{min}}^{\lambda_{max}} I(\lambda) d\lambda} \quad (2)$$

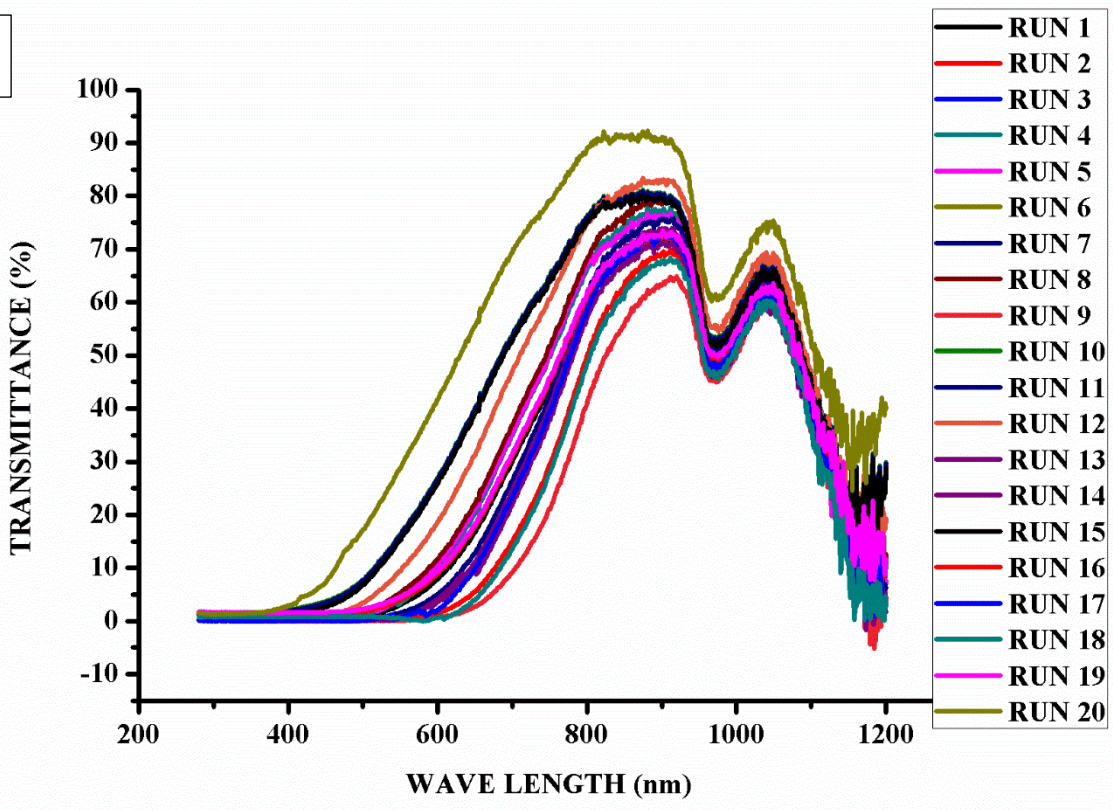
352 Where, A_m is the solar weighted absorption fraction and $I(\lambda)$ is the spectral solar irradiance.
 353 The absorption coefficient ($A(\lambda)$) of the nanofluid was found using the Beer-Lambert Law [25,
 354 26] given by Eq.(3).

$$355 \quad A(\lambda) = -\frac{1}{l} \ln Tr(\lambda) \quad (3)$$

356 where, T_r is the transmittance of nanofluid. The spectrum after the absorption of solar rays was
 357 calculated using the Eq. (4) [27].

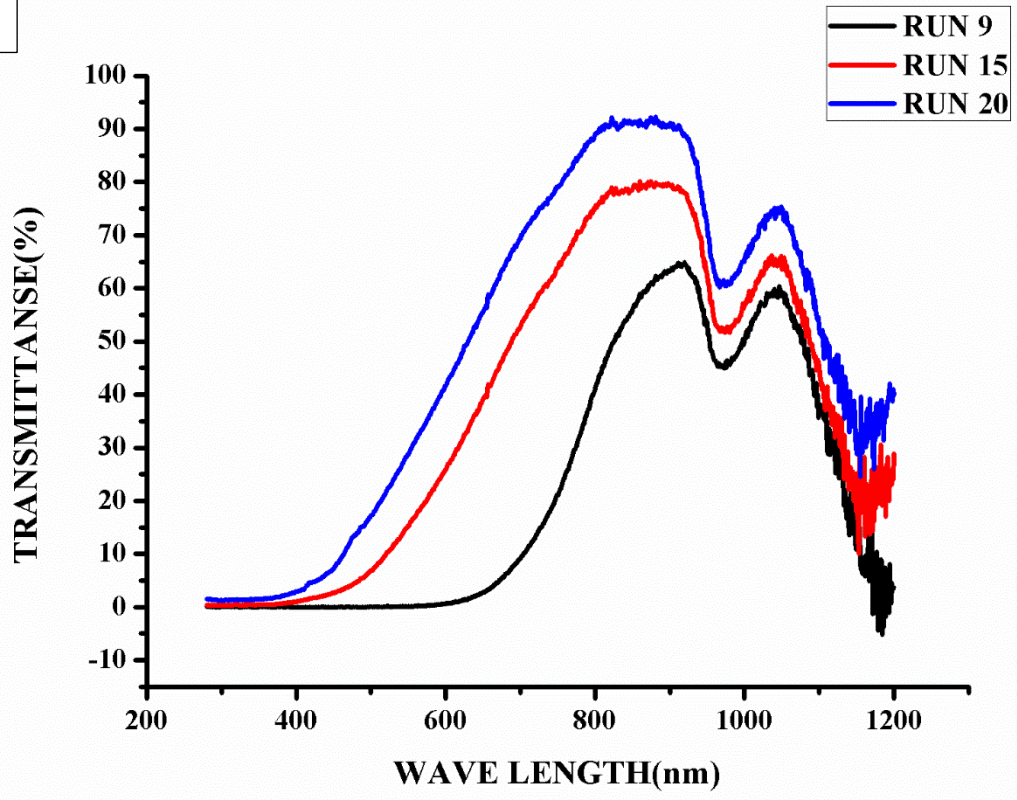
$$358 \quad I_A(\lambda) = A(\lambda) \cdot I_{AM 1.5} \quad (4)$$

a



359

b



360

361 **Fig. 8:** Transmittance spectrum of SiO₂/Ag-CuO nanofluids: a) All runs, b) critical runs

362 From the estimated solar weighted absorption fraction (table 2) it was found that run 9
363 gives the maximum enhancement in the absorption of the nanofluid, whereas run 20 gave the
364 least. These results indicates that the dispersion of SiO₂/Ag-CuO nanoparticles significantly
365 improves the absorption of solar irradiance. Figure 8 shows that the maximum absorption is
366 observed in the range of 280 -750 nm. In addition, a significant amount of absorption is
367 occurring in the spectral range of 900-1050 nm (near inferred region) which is attributed to DI
368 water, a good absorber of infrared rays. Therefore the effect of nanoparticle is significant in the
369 range of 280-750nm.

370 As can be seen from fig 8 run 9 gives the highest solar weighted absorptivity of
371 82.82%, whereas the least value of 50.87 % was observed for run 20. It could be inferred that
372 the surfactant ratio have significance on the solar absorptivity of the nanofluid. At lower
373 concentration of surfactant transmission of the light increased. This could be due to the reduced
374 stability of the nanofluid at lower surfactant concentration leading to sedimentation of particles
375 during the measurement. Nevertheless, this significance of surfactant is of less concern once a
376 stable nanofluid is achieved.

377 3.1.6 ANOVA analysis of solar weighted absorptivity of SiO₂/Ag-CuO nanofluid.

378 The process parameters influencing solar weighted absorption fraction (SWAF) were
379 examined using the ANOVA by response surface methodology (RSM). The process parameters
380 analysed are the concentrations of SiO₂/Ag, CuO, and SDS, which are identified as A, B and
381 C respectively in Table 4. The RSM derived a regression equation (Eq. 5), employing which
382 the solar weighted absorption fraction of the prepared nanofluid could be predicted. The
383 significance of each process parameters on solar absorption were examined using ANOVA.
384 Table 4 shows the analysis of variance of process parameters on solar weighted absorptivity of
385 the SiO₂/Ag-CuO nanofluid. As can be seen from Table 4 the proposed model is found to be
386 significant with a probability (p-value) less than 0.0001 and an insignificant lack of fit (p-value
387 = 0.0545), which implies that the model could predict the SWAF of prepared nanofluid
388 effectively. As mentioned in section 3.1.3, the predicted R² and adjusted R² value are in good
389 agreement so as to adopt the model for prediction of SWAF. A comparison on experimental
390 and predicted value of SWAF is shown in Fig 9. The minimum deviation of experimental
391 values (coloured square point) from the prediction line shows good agreement in the values of
392 SWAF calculated based on theoretical model and using experimental data. The minimum
393 deviation of experimental data points from the prediction line implies that the model is

394 **significant.** The significance of the process parameters are proportional to the F-value obtained
 395 from the ANOVA. The decreasing order of significance is C (mass fraction of surfactant) > A
 396 (mass fraction of SiO₂/Ag) > B (mass fraction of CuO). From Table 2 we can infer that the
 397 only difference between run 18 and 20 is in the concentration of SDS which amounts to 2000
 398 and 100 mg/l respectively for run 18 and 20. Table 2 confirms that run 18 having higher SDS
 399 concentration has better solar absorption than run 20. However, it is the plasmonic effect of
 400 SiO₂/Ag particles that will contribute more towards enhancing SWAF as compared to CuO.
 401 The theoretical model which predicts the SWAF is given by Eq. [5]. Figure 9 shows good
 402 agreement in the values of SWAF calculated based on theoretical model and using
 403 experimental data As mentioned in section 3.1.3, minimum deviation of experimental data
 404 points from the prediction line implies that the model is significant.

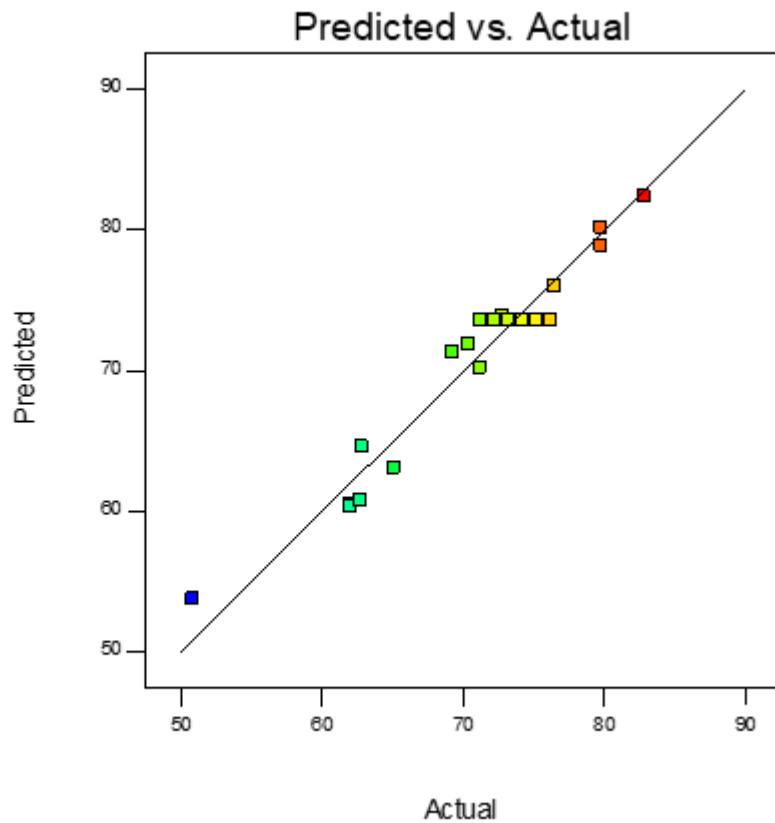
405 Solar weighted absorption fraction = + 35.23790 + (0.021866 X SiO₂/Ag) + (0.010745 X CuO)
 406 + (0.039759 X SDS) - (3.34793E-006 X SiO₂/Ag X CuO) - (6.67764E-006 X SiO₂/Ag X SDS) -
 407 (6.48624E-006 X CuO X SDS) - (1.08898E-005 X SiO₂/Ag²) - (1.95099E-006 X CuO²) -
 408 (7.30303E-006 X SDS²) (5)

409 **Table 4:** ANOVA of solar weighted absorption fraction.

Source	Sum of squares	Df	Mean square	F-value	p-value	
Model	1073.47	9	119.27	22.78	< 0.0001	Significant
A-SiO ₂ /Ag	65.16	1	65.16	12.44	0.0055	
B-CuO	8.23	1	8.23	1.57	0.2384	
C-SDS	840.90	1	840.90	160.59	< 0.0001	
AB	2.69	1	2.69	0.51	0.4898	
AC	19.72	1	19.72	3.77	0.0810	
BC	18.61	1	18.61	3.55	0.0888	
A ²	51.29	1	51.29	9.80	0.0107	
B ²	1.65	1	1.65	0.31	0.5873	
C ²	78.26	1	78.26	14.94	0.0031	
Residual	52.36	10	5.24			
Lack of Fit	34.86	5	6.97	1.99	0.2338	not significant
Pure Error	17.50	5	3.50			
Cor Total	1125.83	19				
Std. Dev.		2.29	R-Squared			0.9535
Mean		70.49	Adj R-Squared			0.9116
C.V. %		3.25	Pred R-Squared			0.7437
PRESS		288.59	Adeq Precision			17.648

410

Color points by value of
SWAF:
82.82
50.87



411

412 **Fig. 9:** Correlation between experimental and predicted values of solar weighted absorption
413 fraction of nanofluid.

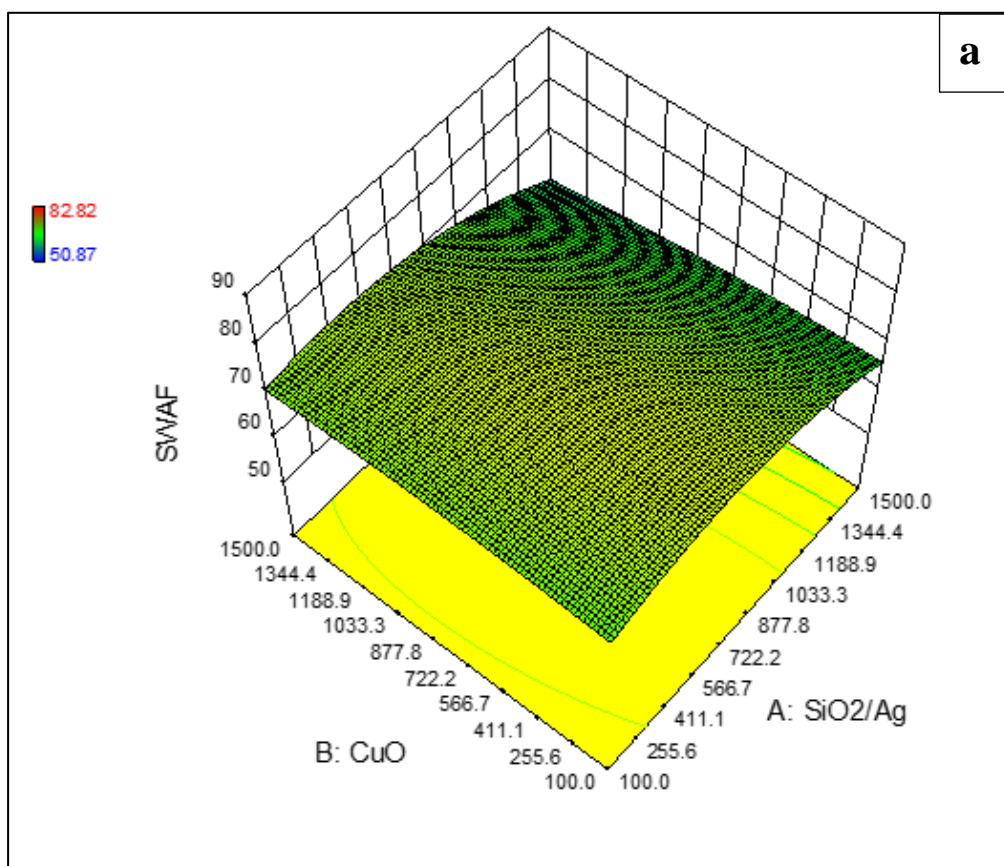
414

415 3.1.7 Interaction effect of particle concentration

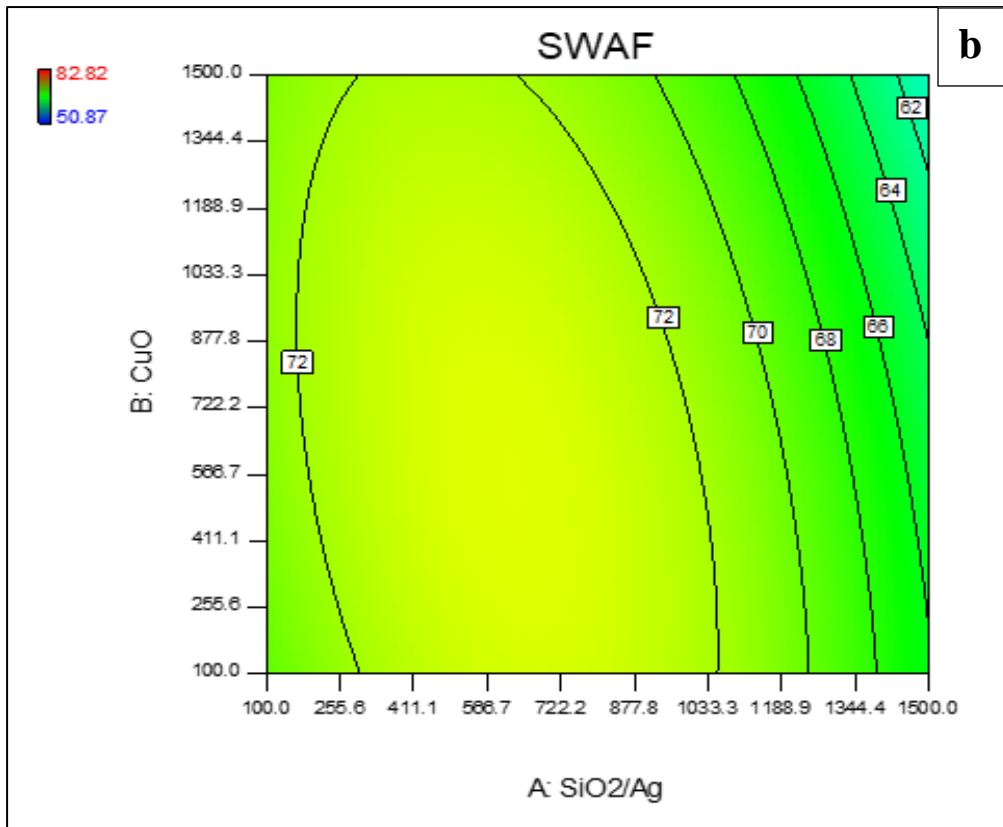
416 Figure 10(a) and 10(b) presents the interaction of SiO₂/Ag and CuO nanoparticle
417 concentration on SWAF of the nanofluid for a given surfactant concentration as a response
418 surface curve and its contour respectively. From the graphs it could be noticed that increase in
419 the concentration of SiO₂/Ag nanoparticles enhanced the solar weighted absorptivity of the
420 nanofluid, reaches a maximum and then drops. The observed range of SiO₂/Ag for maximum
421 solar absorption is 300-800 mg/ litre. The CuO nanoparticles shows maximum solar absorption
422 for the range 100-1000 mg/l. Once the particle concentration exceeds these limits the stability of
423 nanofluids were physically observed to be dropping, resulting in decreased solar absorption. However,
424 the significance of SiO₂/Ag is more compared to CuO. This could be attributed to the surface
425 plasmon resonance effect of Ag nanoparticles on the dielectric SiO₂ particles. Noble metals
426 have the better prospects in absorbing and scattering the light due to its surface plasmon
427 resonance effect [13]. Core shell nanoparticle with dielectric core and noble metal as the shell

428 exhibits better optical absorption compared to pure noble metals [28]. Recently it was proposed
429 that fractal textured surfaces are good candidates for solar absorption due to its increased
430 surface area and scattering of light. In the present work morphology was found to be in a fractal
431 textured manner, which could contribute to enhance light trapping [2].

432 The interaction of surfactant and SiO₂/Ag nanoparticles is presented as a response
433 surface curve and its contour plot in Figure 11(a) and 11(b) respectively. As can be seen from
434 these figure better performance of nanofluid was observed at the highest concentration of
435 surfactant and at a concentration of 750 mg/litre for SiO₂/Ag. For SiO₂/Ag concentration
436 greater than 750 mg/l the stability was observed to be reducing due to the agglomeration of the
437 large SiO₂/Ag particles. A similar trend was noticed in Fig. 12(a) and 12(b) which shows the
438 interaction of CuO and surfactant. That is, the maximum solar weighted absorptivity of
439 nanofluid was observed at higher concentration of surfactant which keeps the particles
440 suspended thus enhances the SWAF. These results also surmise the role of surfactant in
441 improving the properties of the nanofluid by the enhanced stability.



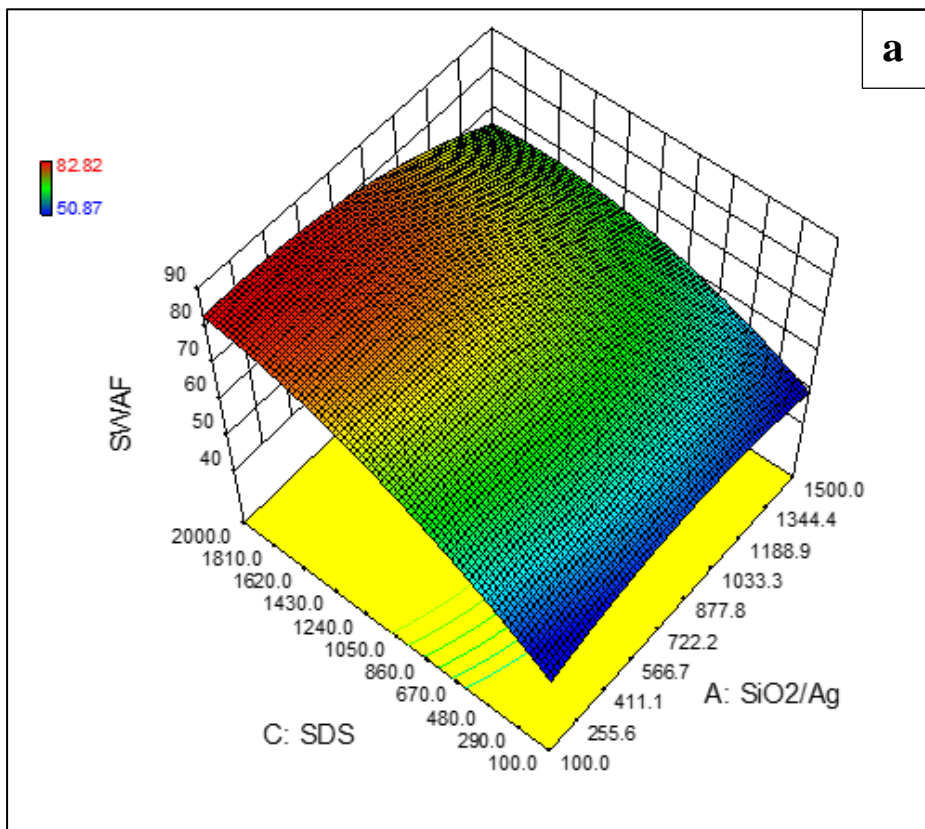
442



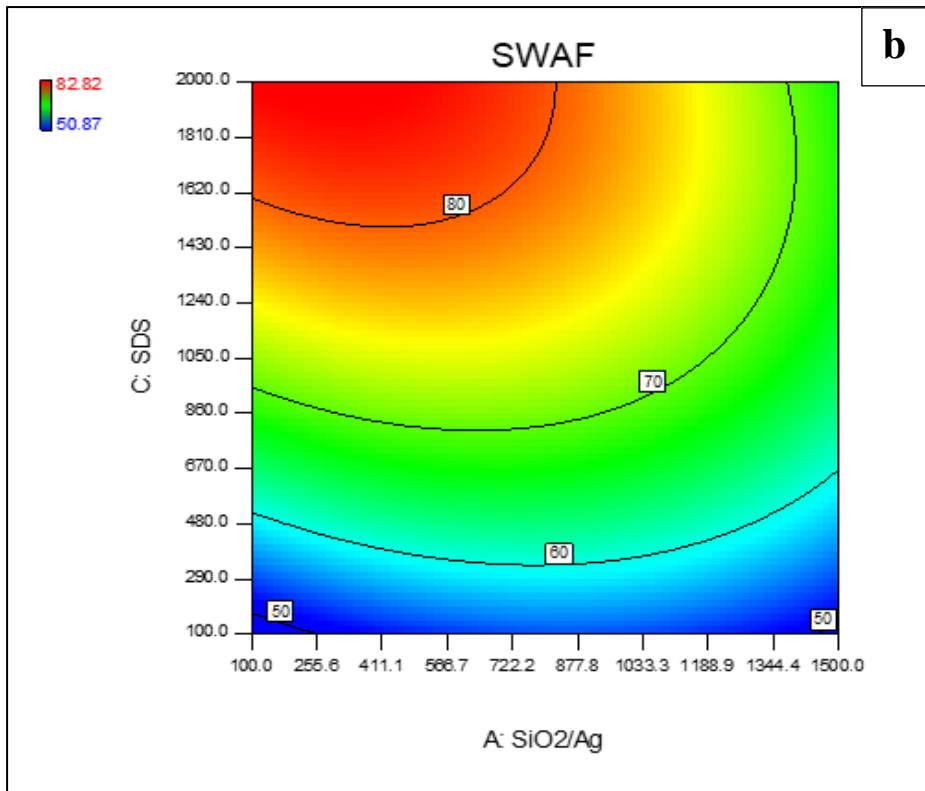
443

444 **Fig. 10:** Interaction effect of mass fraction of SiO₂/Ag and mass fraction of CuO of
 445 nanoparticles on solar weighted absorptivity: a) 3-D graph, b) contour plot.

446



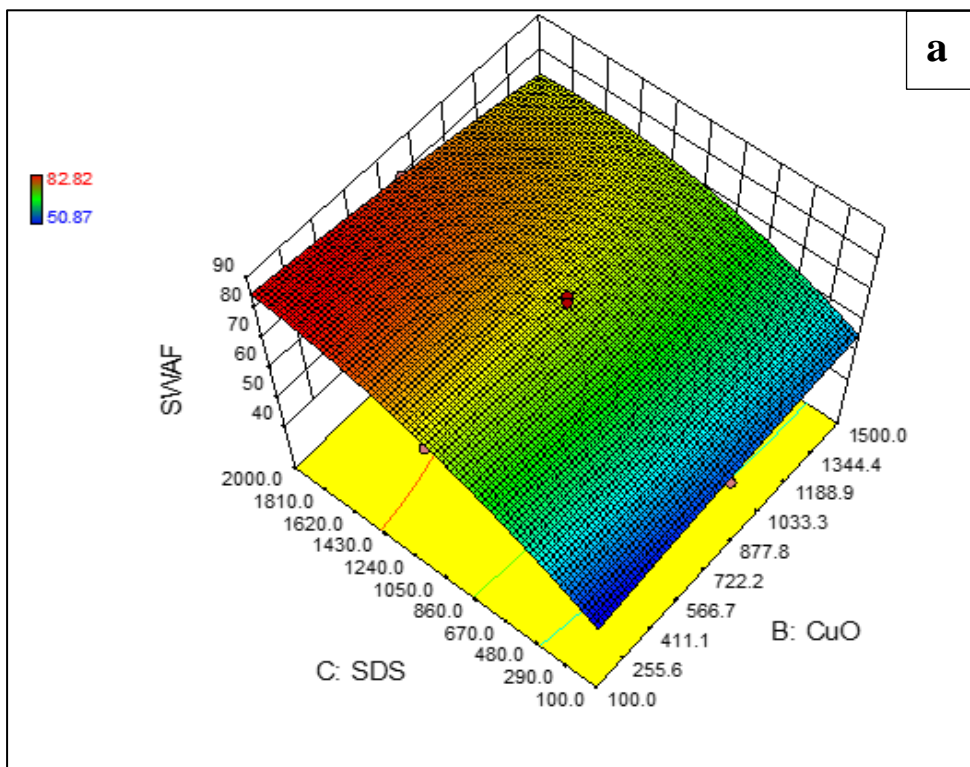
447



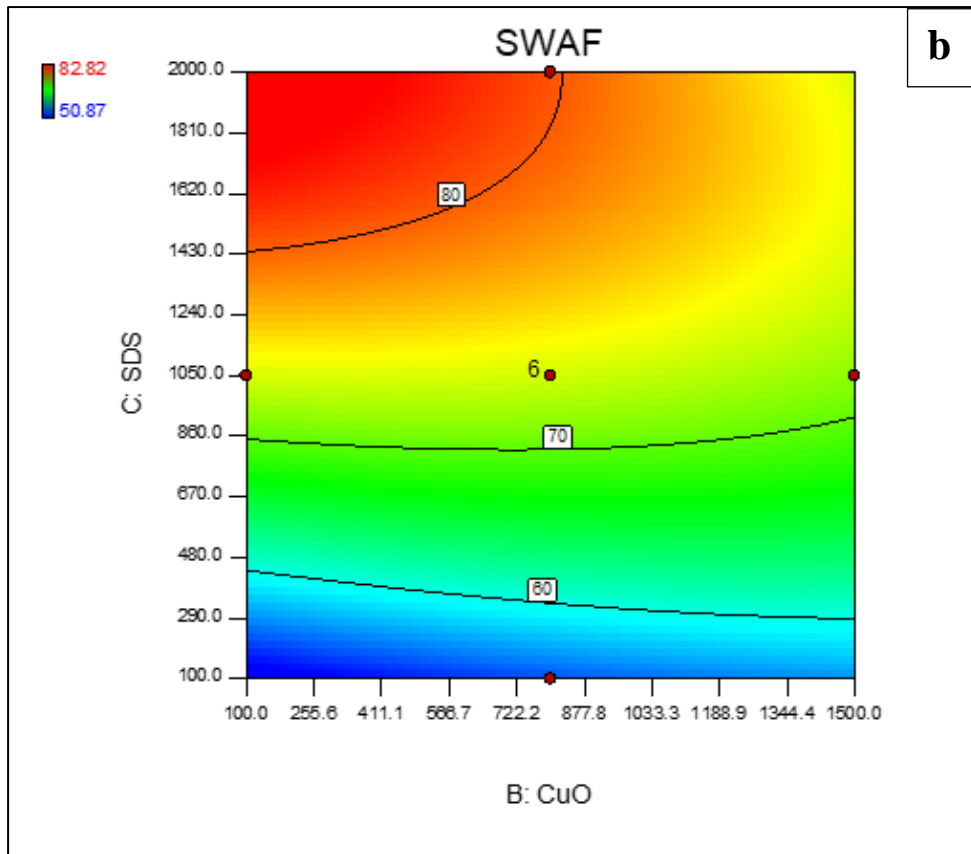
448

449 **Fig. 11:** Interaction effect of mass fraction of SiO₂/Ag and mass fraction of Surfactant of
 450 nanoparticles on solar weighted absorptivity: a) 3-D graph, b) contour plot.

451



452



453

454 **Fig. 12:** Interaction effect of mass fraction of CuO and mass fraction of Surfactant of
 455 nanoparticles on solar weighted absorptivity: a) 3-D graph, b) contour plot.

456 *3.2 Optimisation*

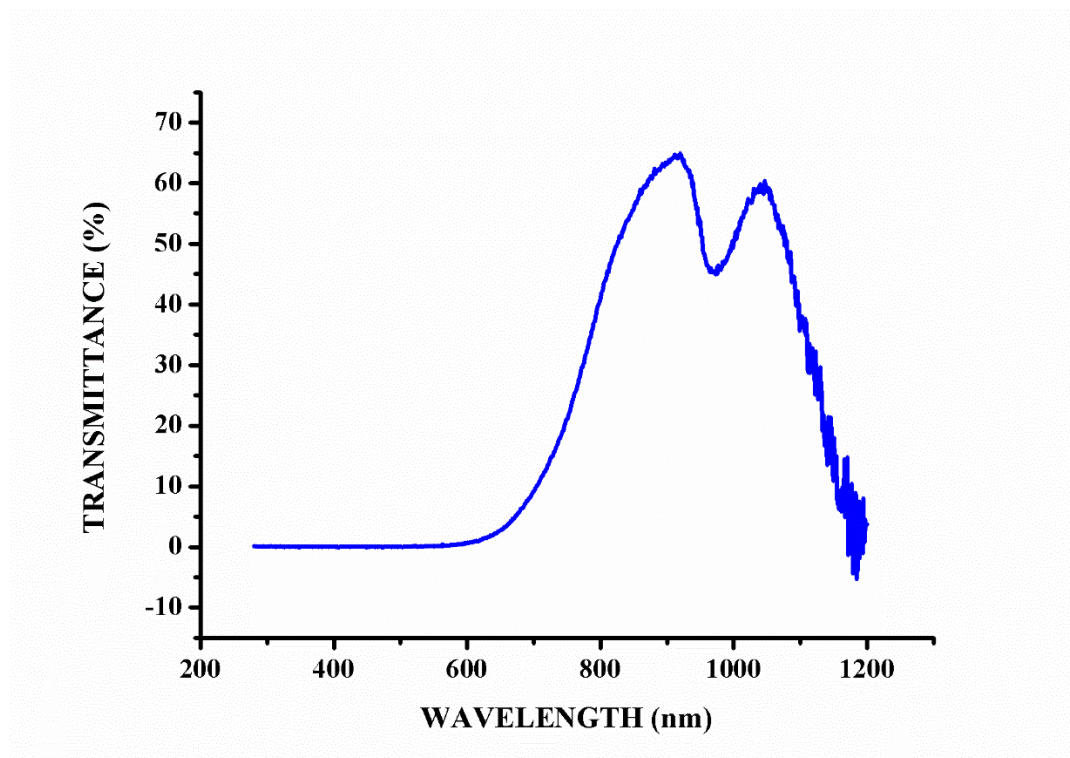
457 In the present study the thermal conductivity and the SWAF are the two properties that
 458 determines the performance of the nanofluid. It is noticed that the constituents in the nanofluid
 459 have greatly affected the thermal and optical properties of the nanofluid. The concentration of
 460 SiO₂/Ag influences SWAF whereas the concentration of CuO improves the thermal
 461 conductivity. Even though solar weighted absorptivity of nanofluid increases with SiO₂/Ag, its
 462 influence on thermal conductivity is inverse. Hence there arises a need to arrive at an optimum
 463 concentration of constituents in the nanofluid so as to achieve better solar absorptivity and
 464 thermal conductivity. One of the main strategy used for optimising these kind multi response
 465 problem is by employing the desirability function. Desirability function employs dimension
 466 reduction strategy in which the multi response model is reduced to a single aggregated measure
 467 and then solves it as a single optimisation problem [30]. Moreover this statistical optimisation
 468 recommends an optimum operating condition of process parameters that maximises the
 469 desirability that range from zero (out of scope) to one (goal) [23]. The condition to obtain an
 470 optimised constitute concentration includes the particle concentration to be in range. The final
 471 optimised parameter is shown in the Table 5. The maximum solar absorptivity of 82.84 % and

472 relative thermal conductivity of 1.234 was found for the concentrations SiO₂/Ag: 206.3
 473 mg/litre, CuO: 864.7 mg/litre and SDS 1996.2 mg/litre. The desirability value 1.000 indicates
 474 that estimated function may represent the experimental model. To verify this experimentally,
 475 relative thermal conductivity (RTC) and SWAF of aforementioned combination of constituents
 476 were measured and was found to be 1.231 and 81.79 respectively. **The UV-vis-NIR**
 477 **transmittance spectrum of optimised nanofluid is presented in Fig 13 form which the SWAF**
 478 **was estimated and is 81.79%.**

479 **Table 5:** Experimental and predicted response at optimised process parameters

Sl No	Mass fraction (mg/l)			Predicted		Experimental	
	SiO ₂ /Ag	CuO	SDS	RTC	SWAF	RTC	SWAF
1	206.3	864.7	1996.2	1.234	82.84	1.231	81.79

480



481

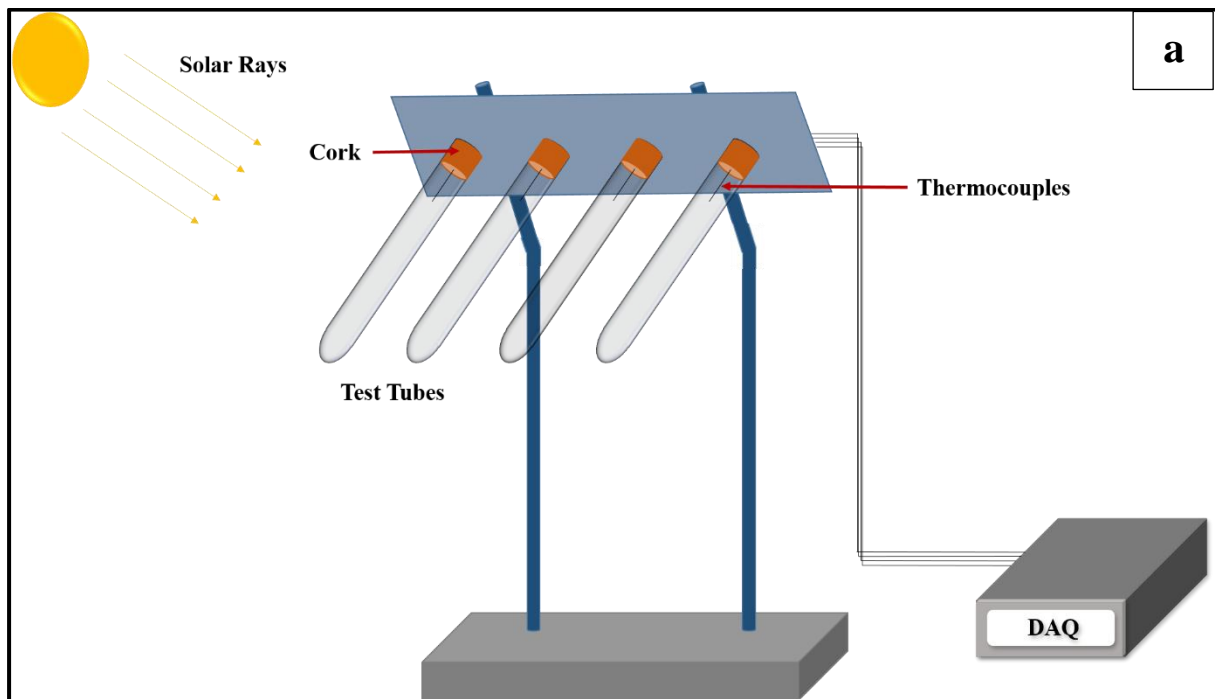
482 **Fig. 13.** Transmittance spectrum of optimised SiO₂/Ag-CuO nanofluids

483 *3.3 Photo-thermal conversion of nanofluid*

484 Even though optical properties propose high solar energy absorption by nanoparticles,
 485 their suitability in solar thermal systems can be quantified only by photo-thermal conversion
 486 studies. The particle concentration in the nanofluid have its own significant effect on the solar

487 absorption. Hence the photo-thermal experiment was conducted using the optimised nanofluid
488 which is then compared to the base fluid.

489 Photo thermal conversion performance of the prepared nanofluid was analysed using an in-
490 house fabricated experimental setup. The experimental setup was equipped with test tubes
491 (27ml) tilted at an angle of 11.3° and mounted on a solid sheet. Figure 14 shows the detailed
492 schematic representation of the arrangement for the same. Figure 14(a) is the schematic
493 representation, Figure 14(b) is the photograph of actual experimental setup, and Figure 14(c)
494 represents tilt angle and dimension of the test tubes. The experimental setup exposed to solar
495 irradiation was fixed in the north-south direction, with the test tubes facing the south. The
496 thermocouples (T Type) were inserted at the centre of the test tubes with the help of a cork
497 fixed at the opening of the test tubes. These were connected to a data logging unit (Agilent),
498 which records the temperature every 5 minutes. The measurements were taken from 10:00
499 16:00.



500

501

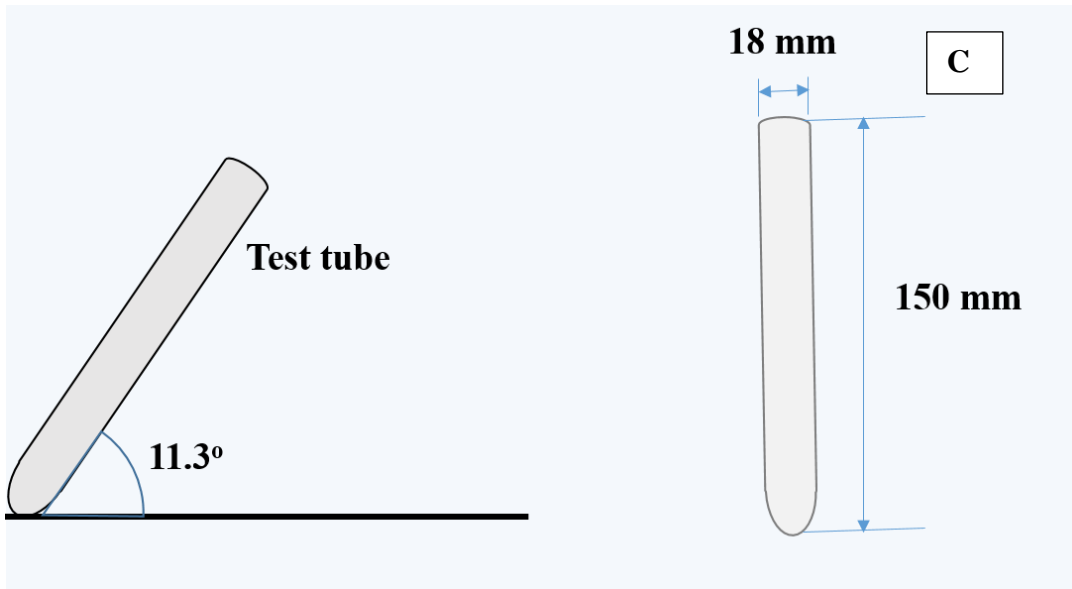
502



b

503

504



c

505

506 **Fig. 14:** Experimental setup for evaluation of photo thermal conversion effect. a) Schematic
 507 representation and b) Actual experimental setup, c) tilt angle and dimension of the test tubes.

508

509 The total energy absorbed by the nanofluid during the photo thermal conversion was
 510 calculated using Eq. 6. The stored energy ratio (SER) quantifies the effect of nanoparticles in
 511 photo thermal conversion and was estimated using Eq. 7 [29].

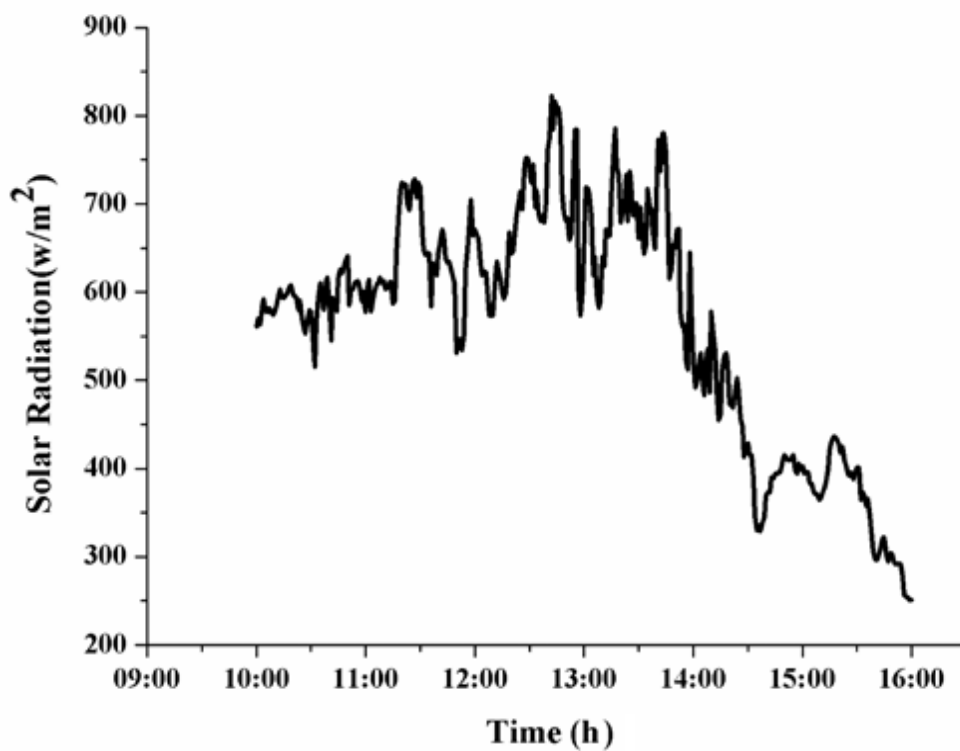
$$512 \quad Q = m.C_p.[T_{\max} - T_{\min}] \tag{6}$$

$$513 \quad SER = \frac{T_{nf}(t) - T_{nf}(0)}{T_{bf}(t) - T_{bf}(0)} \tag{7}$$

514 Where m and c_p are the mass and specific heat of the prepared nanofluid, T is the temperature,
515 and t is the time. Since the concentration of nanoparticles in fluid is comparatively less, the
516 specific heat was equated to be that of water [14].

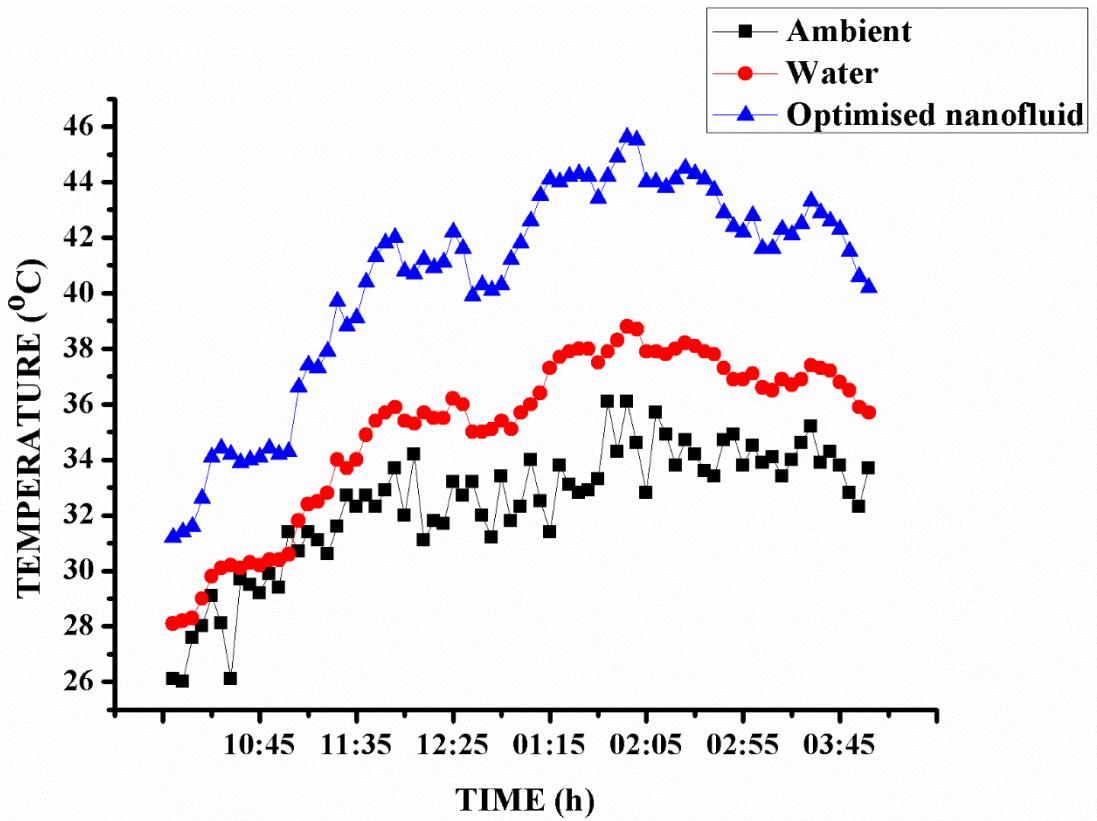
517 Table 6 shows the maximum temperature and the amount of photo thermal energy
518 absorbed by the nanofluid. The solar radiation on the test day given in Fig.15 was obtained
519 from weather station (Davis-Vantage Pro2). As the figure says the solar radiation was 550 w/m^2
520 at 10:00 and 250 w/m^2 during 16:00. A highest irradiance of 850 W/m^2 was noted during the
521 noon time. Figure 16 presents the temperature profile of optimised run compared to base fluid
522 when exposed to the solar radiation. The maximum temperature of optimised nanofluid was
523 45.7°C whereas for water it was 38.8°C . Furthermore the maximum energy was absorbed by
524 nanofluid was 1942.6 J , whereas for water it is 1239 J . Stored energy ratio (SER) enable to
525 identify the supplementary energy absorbed by the fluid due to the presence of nanoparticles
526 which is presented in fig 17. From Fig 17 we can infer that SER increases with the absorption
527 of the nanofluid. Therefore it could be claimed evidently that, the addition of nanoparticles
528 improved the photo-thermal conversion efficiency of the fluid. Heat transfer mechanism in
529 surface based absorption and direct absorption was found to be different. In surface based
530 absorption systems the solar energy is absorbed by the absorber glass and then converted to
531 thermal energy. The thermal energy is then transferred from absorber to the working fluid by
532 conduction and convection [42, 35]. However, in direct absorption systems the solar radiation
533 is absorbed by the nanomaterials dispersed in the base fluid. The penetration of solar radiation
534 lasts to a certain distance or depth termed as penetration depth. The extent of direct absorption
535 of solar energy by base fluid is dependent upon the penetration depth. Variation of SWAF with
536 depth of penetration of the optimised sample is plotted and are presented as fig 18. As can be
537 seen from the figure, nearly 100% of absorption is achieved at a penetration distance of 7cm.
538 The SWAF of water at 7 cm was found to be nearly 30% [27], the penetration depth of the
539 same is nearly 100 cm. From which the complete solar absorption of nanofluid at lower
540 penetration depth is evident. In addition, it is also evident that the working fluids are uniformly
541 heated in direct absorption systems resulting in minimal amount of natural convection heat
542 transfer. Even though natural convection currents at a bulk level are minimal in the working
543 fluid, the energy absorption by the nanomaterials increases their Brownian motion. The
544 enhanced Brownian motion of the particles induces local convection currents and micro-mixing
545 in the fluid for temperature equilibration [39, 40]. In the present case it could also be concluded

546 that the surface plasmon resonance of SiO₂/Ag nanofluid introduced self-heating that enhanced
547 the photo thermal conversion of nanofluid.



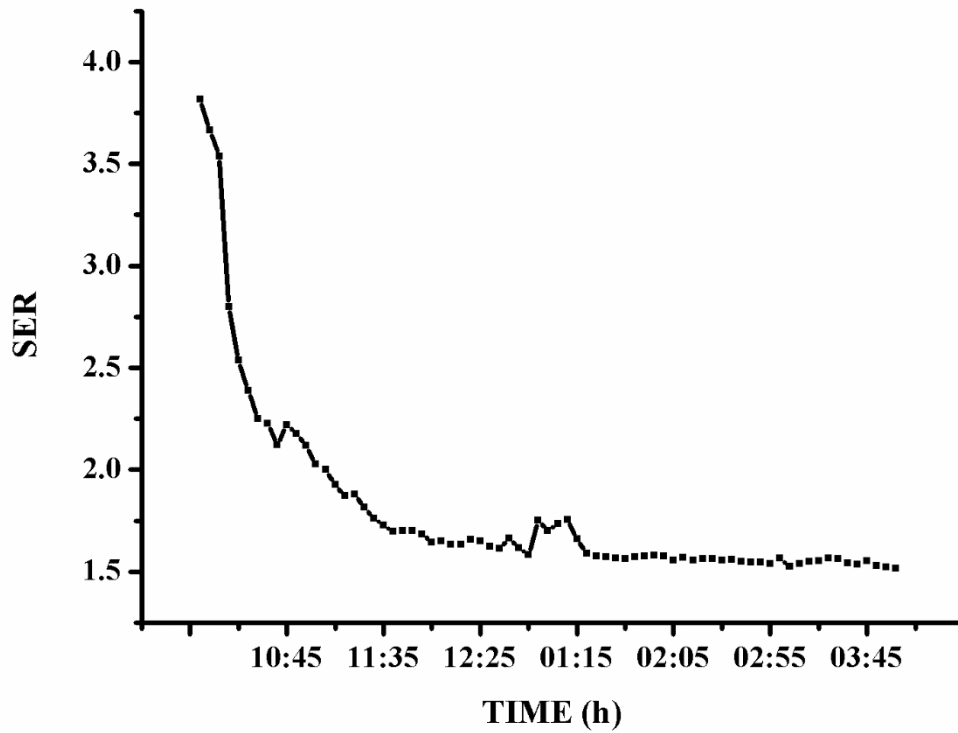
548

549 **Fig. 15:** Solar radiation intensity corresponding to the test day.



550

551 **Fig. 16:** Temperature profile of critical runs and water.



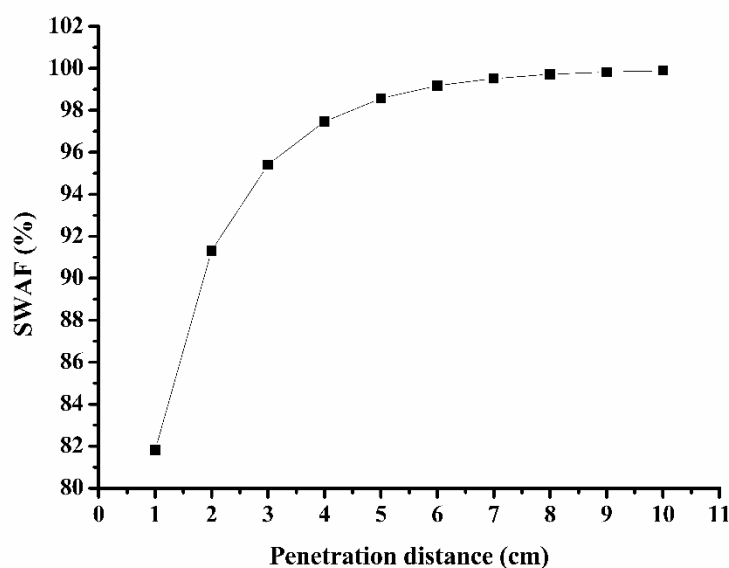
552

553 **Fig. 17:** Stored energy ratio (SER) for the optimised nanofluid

554 **Table 6:** Maximum and minimum fluid temperature and maximum energy absorbed.

Sl. No.	Fluid	T _{max} (°C)	T _{min} (°C)	Energy absorbed (J)
1	Water	38.8	27	1239
2	Optimised nanifluid	45.7	27.1	1942.6

555



556

557 **Fig.18:** Variation of SWAF with depth of penetration.

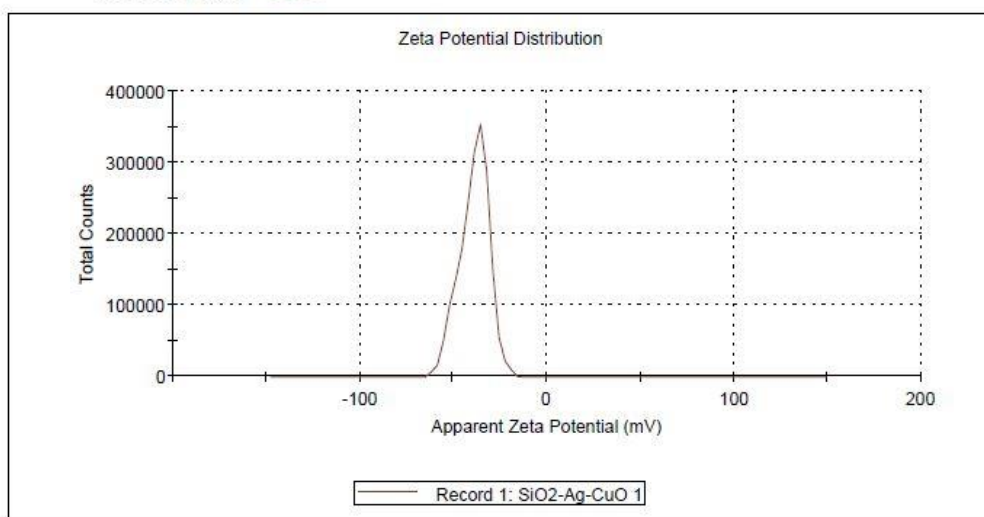
558 3.4 Stability analysis of SiO₂/Ag-CuO nanofluid

559 Stability is one of the major parameter that affects the performance and reliability of
560 the investigations performed on nanofluids. As mentioned in the previous section the thermal
561 conductivity and SWAF reduced for many samples due to the agglomeration of the particles.
562 The surface charges on particles are responsible for the stability of nanofluid owing to the
563 electrostatic repulsive forces between like charged particles. The zeta potential is generally
564 considered as a metric to quantify the stability of electrostatically stabilised nanofluids. The
565 Zeta potential is measured for all the experimental runs in the design matrix and shown in Table
566 7. The Zeta potential of optimised sample was measured and was found to be -38.7 mV. Figure
567 19 shows the zeta potential curve of the same which was obtained from the zeta potential
568 analyser. The result indicates good colloidal stability of the optimised nanofluid, since a stable

569 nanofluid exhibits the zeta potential is below -30 mV or above +30mV. Moreover even though
 570 run 9 exhibits nearly similar zeta potential as the optimised sample, better thermo-optical
 571 properties are shown by the optimised sample. However it is reported that, in a flow situation
 572 of nanofluids the stability could be achieved by means of flow stirring [13] as is present in
 573 various direct absorption solar thermal devices like parabolic collector, flat plate collector, etc.
 574

Results

	Mean (mV)	Area (%)	St Dev (mV)
Zeta Potential (mV): -38.7	Peak 1: -38.7	100.0	7.77
Zeta Deviation (mV): 7.77	Peak 2: 0.00	0.0	0.00
Conductivity (S/m): 0.0570	Peak 3: 0.00	0.0	0.00
Result quality Good			



575

576 **Fig 19.** Zeta potential of optimised SiO₂/Ag-CuO nanofluid.

577 **Table. 7** Zeta potential of experimental runs in the design matrix

Run	Zeta potential (mV)	Run	Zeta potential (mV)
1	21.2	11	18.4
2	29.1	12	20.3
3	30.6	13	27.2
4	26.3	14	20.3
5	20.1	15	21.7

6	16.3	16	28.7
7	21.9	17	22.9
8	22.1	18	28.7
9	33.7	19	21.6
10	22.9	20	14.5

578

579

580 **4. Conclusion**

581 The nanofluid containing SiO₂/Ag and CuO was prepared to enhance the thermal
582 conductivity and solar absorption for direct absorption solar thermal solar collectors. Thermal
583 and optical properties of SiO₂/Ag –CuO nanofluid were measured and the process parameters
584 were optimised using the design of experiment concept. The results reveal that the presence of
585 CuO improves the thermal conductivity where are the plasmonic SiO₂/Ag particles are good in
586 absorbing solar irradiance. The stability of nanofluids strongly influence the thermal and
587 optical properties of the nanofluid. The concentration of surfactant have a great significance in
588 both thermal and optical properties. Maximum solar weighted absorption of 82.84 % was noted
589 for run 9 (SiO₂/Ag: CuO: SDS = 383.3: 383.3: 1614.9) and highest measured thermal
590 conductivity of 1.234 was noted for run 2 (SiO₂/Ag: CuO: SDS = 383.3: 1216.2: 1614.9). The
591 photo thermal conversion effect increased with the absorptivity of nanofluid. To optimise the
592 process parameters like particle concentration and surfactant ratio, desirability function was
593 used. An optimum condition of 206.3 mg/l of SiO₂/Ag, 864.7 mg/l CuO, and 1996.2 mg/l of
594 SDS was found with desirability of 1.000. A significant regression model has been developed
595 to predict the RTC and SWAF of prepared nanofluid. The significance of the model and process
596 parameters on thermal conductivity and solar weighted absorption fraction was ensured using
597 analysis of variance (ANOVA).

598 **References**

- [1] R. Sioshansi, P. Denholm, The value of concentrating solar power and thermal energy storage, *IEEE Trans. Sustain. Energy* 1 (2010) 173–183 <https://doi.org/10.1109/TSTE.2010.2052078>
- [2] R. Jain, R. Pitchumani, Fabrication and characterization of multiscale, fractal textured solar selective coatings, *Sol. Energy Mater. Sol Cells* 172 (2017) 213–219 <https://doi.org/10.1016/j.solmat.2017.07.009>

- [3] Ricardo Vasquez Padilla, Gokmen Demirkaya, D. Yogi Goswami, Elias Stefanakos, Muhammad M. Rahmane, Heat transfer analysis of parabolic trough solar receiver, *Appl. Energy* 88 (12) (2011) 5097-5110
<https://doi.org/10.1016/j.apenergy.2011.07.012>
- [4] M.H. Gray, R. Tirawat, K.A. Kessinger, P.F. Ndione, High temperature performance of high-efficiency, multi-layer solar selective coatings for tower applications, *Energy Procedia* 69 (2015) 398-404 <https://doi.org/10.1016/j.egypro.2015.03.046>
- [5] B.A.J. Rose, H. Singh, N. Verma, S. Tassou, S. Suresh, N. Anantharaman, D. Mariotti, P. Maguire, Investigations into nanofluids as direct solar radiation collectors, *Sol. Energy* 147 (2017) 426-431
<https://doi.org/10.1016/j.solener.2017.03.063>
- [6] P. Phelan, T. Otonicar, R. Taylor, H. Tyagi, Trends and opportunities in direct absorption solar thermal collectors, *J. Therm. Sci. Eng. Appl.* 5 (2013) 21003- 21012
<https://doi.org/10.1115/1.4023930>
- [7] Ismail W. Almanassra, Abdallah D. Manasrah, Usamah A. Al- Mubaiyedh, Tareq Al-Ansari, Zuhair Omar Malaibari, Muataz A. Atieh, An experimental study on stability and thermal conductivity of water/CNTs nanofluids using different surfactants: A comparison study. *J. Mol. Liq.* 22 (2019) 111025
<https://doi.org/10.1016/j.molliq.2019.111025>
- [8] A. Mwesigye, J.P. Meyer, Optimal thermal and thermodynamic performance of a solar parabolic trough receiver with different nanofluids and at different concentration ratios, *Appl. Energy* 193 (2017) 393–413
<https://doi.org/10.1016/j.apenergy.2017.02.064>
- [9] Jotham Muthoka Munyalo, Xuelai Zhang, Particle size effect on thermophysical properties of nanofluid and nanofluid based phase change materials: A review, *J. Mol. Liq.* 265 (2018) 77–87
<https://doi.org/10.1016/j.molliq.2018.05.129>
- [10] Gómez-Villarejo R, Martín EI, Navas J, Sánchez-Coronilla A, Aguilar T, Gallardo JJ, Ag-based nanofluidic system to enhance heat transfer fluids for concentrating solar power: nano-level insights, *Appl. Energy* 194 (2017) 19–29
<https://doi.org/10.1016/j.apenergy.2017.03.003>
- [11] Sarkar J, Ghosh P, Adil A, A review on hybrid nanofluids: recent research, development and applications, *Renew Sustain Energy Rev* 43 (2015) 164–177
<https://doi.org/10.1016/j.rser.2014.11.023>
- [12] Hamza Babar, Hafiz Muhammad Ali, Towards hybrid nanofluids: Preparation, thermophysical properties, applications, and challenges, *J. Mol. Liq.* 281 (2019) 598–633
<https://doi.org/10.1016/j.molliq.2019.02.102>
- [13] Xiaoxiao Yu, Yimin Xuan, Investigation on thermo-optical properties of CuO/Ag plasmonic nanofluids, *Sol. Energy* 160 (2018) 200-207
<https://doi.org/10.1016/j.solener.2017.12.007>
- [14] Jia Zeng, Yimin Xuan, Enhanced solar thermal conversion and thermal conduction of MWCNT-SiO₂/Ag binary nanofluids, *Appl. Energy*, 212 (15) (2018), 809-819
<https://doi.org/10.1016/j.apenergy.2017.12.083>
- [15] Pawel Koblinski, Jeffrey A. Eastman, David G. Cahill, Nanofluid for thermal transport, *Mater. Today*, 8 (6) (2005) 36-44
[https://doi.org/10.1016/S1369-7021\(05\)70936-6](https://doi.org/10.1016/S1369-7021(05)70936-6)
- [16] A.H. Elsheikh, S.W. Sharshir, Mohamed. Mostafa, F.A. Essa, Mohamed Kamal Ahmed Ali, Applications of nanofluids in solar energy: A review of recent advances,

- renewable and sustainable energy rev, 82 (2018) 3483–3502
<https://doi.org/10.1016/j.rser.2017.10.108>
- [17] Liu Z-H, Hu R-L, Lu L, Zhao F, Xiao H-s, Thermal performance of an open thermosiphon using nanofluid for evacuated tubular high temperature air solar collector, Energy Convers Manag, 73 (2013) 135–143
<https://doi.org/10.1016/j.enconman.2013.04.010>
- [18] S.P. Sivapirakasam, M. Sreejith, M.C. Santhosh Kumar, M. Surianarayanan, Welding fume reduction by nano-alumina coating on electrodes - towards green welding process, J. Cleaner Prod.108 (2015) 131-144
<https://doi.org/10.1016/j.jclepro.2015.06.132>
- [19] Werner stober, Arthur Fink, Ernest Bohn, Controlled growth of monodisperse silica spheres in the micron size range, J. colloid and Interface Sci 26 (1968) 62-69
[https://doi.org/10.1016/0021-9797\(68\)90272-5](https://doi.org/10.1016/0021-9797(68)90272-5)
- [20] Karen Cacia, Robison Buitrago-Sierra, Bernardo Herrera, Farid Chejne, Elizabeth Pabón, Influence of different parameters and their coupled effects on the stability of alumina nanofluids by a fractional factorial design approach, Adv. Power Technol. 28 (2017) 2581-2588
<https://doi.org/10.1016/j.appt.2017.07.009>
- [21] Albin Joseph, Sreejith Mohan, C.S. Sujith Kumar, Arun Mathew, Shijo Thomas, B.R. Vishnu, S.P. Sivapirakasam, An experimental investigation on pool boiling heat transfer enhancement using sol-gel derived nano-CuO porous coating, Exp. Therm Fluid Sci.103 (2019) 37-50
<https://doi.org/10.1016/j.expthermflusci.2018.12.033>
- [22] Mohammad Hemmat Esfe, Masoumeh Firouzi, Hossein Rostamian, Masoud Afrand. Prediction and optimization of thermophysical properties of stabilized Al₂O₃/antifreeze nanofluids using response surface methodology, J. Mol. Liq. 261 (2018) 14-20
<https://doi.org/10.1016/j.molliq.2018.03.063>
- [23] Payman Davoodi-Nasab, Ahmad Rahbar-Kelishami, Jaber Safdari, Hossein Abolghasemi. Application of emulsion nanofluids membrane for the extraction of gadolinium using response surface methodology, J. Mol. Liq. 244 (2017) 368-373
<https://doi.org/10.1016/j.molliq.2017.08.127>
- [24] W.D. Drotning, Optical properties of solar-absorbing oxide particles suspend in a molten salt heat transfer fluid, Sol. Energy 20 (1978) 313–319
[https://doi.org/10.1016/0038-092X\(78\)90123-8](https://doi.org/10.1016/0038-092X(78)90123-8)
- [25] T.B. Gorji, A.A. Ranjbar, S.N. Mirzababaei, Optical properties of carboxyl functionalized carbon nanotube aqueous nanofluids as direct solar thermal energy absorbers, Sol. Energy 119 (2015) 332–342
<https://doi.org/10.1016/j.solener.2015.07.012>
- [26] N. Hordy, D. Rabilloud, J.L. Meunier, S. Coulombe, High temperature and long term stability of carbon nanotube nanofluids for direct absorption solar thermal collectors, Sol. Energy 105 (2014) 82–90
<https://doi.org/10.1016/j.solener.2014.03.013>
- [27] Nan Chen, Haiyan Ma, Yang Li, Jinhua Cheng, Canying Zhang, Daxiong Wu, Haitao Zhu. Complementary optical absorption and enhanced solar thermal conversion of CuO-ATO nanofluids, Sol. Energy Mater. Sol Cells. 162 (2017) 83-92
<https://doi.org/10.1016/j.solmat.2016.12.049>
- [28] Taylor RA, Otanicar TP, Herukerrupu Y, Bremond F, Rosengarten G, Hawkes ER, Feasibility of nanofluid-based optical filters, Appl Opt 52 (2013) 1413–1422
<https://doi.org/10.1364/AO.52.001413>

- [29] Carolina L.L. Beicker, Muhammad Amjad, Enio P. Bandarra Filho, Dongsheng Wen, Experimental study of photothermal conversion using gold/water and MWCNT/water nanofluids, *Sol. Energy Mater. Sol. Cells* 188 (2018) 51–65
<https://doi.org/10.1016/j.solmat.2018.08.013>
- [30] Dong Hee Lee, In Jun Jeong, Kwang Jae Kim, A desirability function method for optimizing mean and variability of multiple responses using a posterior preference articulation approach, *Qual. Reliab. Eng. Int* 24 (3) (2018) 360–376
<https://doi.org/10.1002/qre.2258>
- [31] M.N. Hyder, R.Y.M. Huang, P. Chen, Pervaporation dehydration of alcohol water mixtures: optimization for permeate flux and selectivity by central composite rotatable design, *J. Membr. Sci.* 326 (2009) 343–353
<https://doi.org/10.1016/j.memsci.2008.10.014>
- [32] Mohammad Mustafa Ghafurian, Hamid Niazmand, Fateme Tavakoli Dastjerd, Omid Mahian, A study on the potential of carbon-based nanomaterials for enhancement of evaporation and water production, *Chem. Eng. Sci* 207 (2019) 79–90.
<https://doi.org/10.1016/j.ces.2019.05.043>
- [33] Saman Rashidi, Nader Karimi, Omid Mahian, Javad Abolfazli Esfahani, A concise review on the role of nanoparticles upon the productivity of solar desalination systems, *J. therm. Anal. Calorim* (2019) 135:1145–1159.
- [34] Nipun Goel, Robert A. Taylor, Todd Otanicar, A review of nanofluid-based direct absorption solar collectors: Design considerations and experiments with hybrid PV/Thermal and direct steam generation collectors, *Renewable Energy* 145 (2020) 903–913
<https://doi.org/10.1016/j.renene.2019.06.097>
- [35] Vishal Bhalla, Sachin Beejawat, Jay Doshi, Vikrant Khullar, Harjit Singh, Himanshu Tyagi, Silicone oil envelope for enhancing the performance of nanofluid based direct absorption solar collectors. *Renewable energy* 145 (2020) 2733:2740.
<https://doi.org/10.1016/j.renene.2019.08.024>
- [36] Amin Asadi, Farzad Pourfattah, Imre Miklos Szilagyi, Masoud Afrand, Gawel Żyła, Ho Seon Ahn, Somchai Wongwises, Hoang Minh Nguyen, Ahmad Arabkoohsar, Omid Mahian, Effect of sonication characteristics on stability, thermophysical properties, and heat transfer of nanofluids: A comprehensive review, *Ultrason. Sonochem* 58 (2019) 104701
<https://doi.org/10.1016/j.ultsonch.2019.104701>
- [37] Caiyan Qin, Joong Bae Kim, Hiroki Gonome, Bong Jae Lee, Absorption characteristics of nanoparticles with sharp edges for a direct-absorption solar collector, *Renewable Energy* 145 (2020) 21–28
<https://doi.org/10.1016/j.renene.2019.05.133>
- [38] Omid Mahian, Lioua Kolsi, Mohammad Amani, Patrice Estelle, Goodarz Ahmadi, Clement Kleinstreuer, Jeffrey S. Marshall, Majid Siavashi, Robert A. Taylor, Hamid Niazmand, Somchai Wongwises, Tasawar Hayat, Arun Kolanjiyil, Alibakhsh Kasaeian, Ioan Pop, Recent advances in modeling and simulation of nanofluid flows—Part I: Fundamentals and theory, *Phys. Rep* 790 (2019) 1–48.
<https://doi.org/10.1016/j.physrep.2018.11.004>
- [39] Omid Mahian, Lioua Kolsi, Mohammad Amani, Patrice Estelle, Goodarz Ahmadi, Clement Kleinstreuer, Jeffrey S. Marshall, Robert A. Taylor, Eiyad Abu-Nada, Saman Rashidi, Hamid Niazmand, Somchai Wongwises, Tasawar Hayat, Alibakhsh Kasaeian, Ioan Pop, Recent advances in modelling and simulation of nanofluid flows—Part II: Applications, *Phys. Rep* 791 (2019) 1–59
<https://doi.org/10.1016/j.physrep.2018.11.003>

- [40] Y. Feng, C. Kleinstreuer, Nanofluid convective heat transfer in a parallel-disk system, *Int. J. Heat Mass Transfer* 53 (2010) 4619–4628.
<https://doi.org/10.1016/j.ijheatmasstransfer.2010.06.031>
- [41] Mikko Makela, Experimental design and response surface methodology in energy applications: A tutorial review, *Energy Convers. Manage* 151 (2017) 630–640.
<https://doi.org/10.1016/j.enconman.2017.09.021>
- [42] Salma Parvin, Rehana Nasrin, M.A. Alim, Heat transfer and entropy generation through nanofluid filled direct absorption solar collector, *Int J. Heat Mass Transfer* 71 (2014) 386–395.
<https://doi.org/10.1016/j.ijheatmasstransfer.2013.12.043>
- [43] M.M.Sarafraz, Mohammad Reza Safaei, Diurnal thermal evaluation of an evacuated tube solar collector (ETSC) charged with graphene nanoplatelets-methanol nanosuspension, *Renewable energy* 142 (2019) 364–372.
<https://doi.org/10.1016/j.renene.2019.04.091>
- [44] Janki Shah, Saket Kumar, Mukesh Ranjan, Yogesh Sonvane, Prachi Thareja, Sanjeev K. Gupta, The effect of filler geometry on thermo-optical and rheological properties of CuO nanofluid, *J. Mol. Liq.* 272 (2018) 668–675
<https://doi.org/10.1016/j.molliq.2018.09.117>
- [45] Debing Wang, Yanlin Jia, Yan He, Lingling Wang, Jinghong Fan, Huaqing Xie, Wei Yu, Enhanced photothermal conversion properties of magnetic nanofluids through rotating magnetic field for direct absorption solar collector, *J. Colloid Interface Sci.* 557 (2019) 266–275
<https://doi.org/10.1016/j.jcis.2019.09.022>
- [46] S.K. Hazra, S. Ghosh, T.K. Nandi, Photo-thermal conversion characteristics of carbon black-ethylene glycol nanofluids for applications in direct absorption solar collectors, *Appl. Therm. Eng.* 163 (2019) 114402
<https://doi.org/10.1016/j.applthermaleng.2019.114402>
- [47] Kongxiang Wang, Yan He, Ankang Kan, Wei Yu, Debing Wang, Liyie Zhang, Guihua Zhu, Huaqing Xie, Xiaohui She, Significant photothermal conversion enhancement of nanofluids induced by Rayleigh-Benard convection for direct absorption solar collectors, *Appl. Energy* 254 (2019) 113706
<https://doi.org/10.1016/j.apenergy.2019.113706>
- [48] Omar Z. Sharaf, Nahla Rizk, Chakra P. Joshi, Maguy Abi Jaoude, Ashraf N. Al-Khateeb, Dimitrios C. Kyritsis, Eiyad Abu-Nada, Matthew N. Martin, Ultrastable plasmonic nanofluids in optimized direct absorption solar collectors, *Energy Convers Manag*, 199 (2019) 112010.
<https://doi.org/10.1016/j.enconman.2019.112010>